Author Manuscript

Author Manuscript

Author Manuscript

Author Manuscript

HHS Public Access

Author manuscript

Cancer Res. Author manuscript; available in PMC 2025 November 18.

Published in final edited form as:

Cancer Res. 2025 May 02; 85(9): 1708–1724. doi:10.1158/0008-5472.CAN-24-2492.

Stabilization of RUNX1 Induced by O-GlcNAcylation Promotes PDGF-BB-Mediated Resistance to CDK4/6 Inhibitors in Breast Cancer

Shuyan Zhou[1,7], **Yi Zhang**[1,7,*], **Julie Belmar**[4], **Chunyan Hou**[2], **Yaqin Zhang**[3], **Changmin Peng**[1], **Yunxiao Meng**[6], **Zhuqing Li**[1], **Muhammad Jameel Mughal**[1], **Yanjun Gao**[1], **Edward Seto**[1], **Min Shen**[3], **Matthew D Hall**[3], **Junfeng Ma**[2], **Cynthia X. Ma**[5], **Shunqiang Li**[4,*], **Wenge Zhu**[1,8,*]

[1]Department of Biochemistry and Molecular Medicine, GWU Cancer Center, George Washington University School of Medicine and Health Sciences, Washington, DC 20052, USA.

[2]Department of Oncology, Lombardi Comprehensive Cancer Center, Georgetown University Medical Center, Washington, DC 20057, USA.

[3]Division of Preclinical Innovation, National Center for Advancing Translational Sciences (NCATS), National Institutes of Health (NIH), Rockville, MD 20850, USA.

[4]Department of Medicine, Washington University School of Medicine in St Louis, Siteman Cancer Center, St Louis, MO 63110, USA.

[5]Division of Oncology, Department of Internal Medicine, Washington University School of Medicine in St Louis, St. Louis, MO 63110, USA

[6]Laboratory & Molecular and Genomic Pathology, Department of Laboratory and Transfusion Services, The George Washington University Hospital, Washington, DC 20052, USA.

[7]These authors contributed equally

[8]Lead Contact

Abstract

Cyclin-dependent kinases 4 and 6 (CDK4/6) are crucial in regulating cell cycle progression and cancer development. Targeting CDK4/6 has shown considerable promise in treating various cancers, including breast cancer. Despite significant therapeutic efficacy, resistance to CDK4/6 inhibitors (CDK4/6i), such as palbociclib, remains a substantial hurdle in clinical practice. Using a co-culture system, cytokine array, and quantitative high-throughput combinatorial screening

*Corresponding author: Wenge Zhu, wz6812@gwu.edu; Yi Zhang, scholarzy@gwu.edu, 800 22ND ST NW, Science and Engineering Hall, Room 8480, Washington DC, 20037. Shunqiang Li, shunqiangli@wustl.edu, 4515 McKinley Ave, Couch Biomedical Research Bldg, Room 3307, St. Louis, MO 63110.

AUTHOR CONTRIBUTIONS

S.Z. drafted the paper and performed most of the experiments with assistance from Y.Z., J.B., C.P., E.S., Z.L., M.JM. and Y.G.. Y.M. assisted with pathological analysis of the slides. C.H. and J.M. designed and performed the mass spectrometry analysis. M.H., Y.Z. and M.S. designed and performed the high-throughput drug screening assay. S.L. and C.M. provided the clinical patient samples. W.Z. supervised the project, co-wrote the manuscript, provided experimental advice, and obtained funding to support the project.

COMPETING INTERESTS

The authors declare no competing interests

Author Manuscript Author Manuscript Author Manuscript Author Manuscript

(qHTCS), we discovered a mechanism by which the RUNX1-PDGF-BB axis regulates palbociclib resistance in breast cancer cells. Specifically, RUNX1 functioned as a transcription factor to drive expression of PDGF-BB, leading to resistance to palbociclib by enhancing the Akt pathway and suppressing senescence. Furthermore, in resistant cells, RUNX1 was O-GlcNAcylated at serine 252 (S252) by OGT, resulting in the stabilization of RUNX1 by preventing ubiquitin-mediated degradation. Inhibition of the RUNX1-PDGF-BB axis by specific inhibitors overcame palbociclib resistance both in vitro and in vivo. Notably, the RUNX1-PDGF-BB axis was upregulated in resistant patient-derived xenograft (PDX) lines and in breast cancer patients following treatment with CDK4/6i. These findings not only unveil O-GlcNAcylation-mediated activation of a RUNX1-PDGF-BB pathway as a driver of palbociclib resistance but also provide clinical evidence supporting the repurposing of FDA-approved PDGFR inhibitors as a therapeutic strategy to treat CDK4/6i-resistant breast cancer patients.

INTRODUCTION

The cyclin-dependent kinase (CDK) 4 and 6 are enzymes that form complexes with cyclin D proteins to phosphorylate the retinoblastoma protein (Rb), leading to its inactivation and the subsequent release of E2F, which promotes the expression of genes necessary for cell cycle progression from G1 to S phase (1). Dysregulation of CDK4/6 activity can lead to uncontrolled cell proliferation, tumor growth, and progression (2). Targeting CDK4/6 has emerged as a promising approach for cancer therapy. Currently, three CDK4/6 inhibitors (CDK4/6i), palbociclib, ribociclib and abemaciclib, have been approved by FDA for use in combination with endocrine therapy, especially for hormone receptor-positive breast cancer (3). Moreover, CDK4/6i has exhibited promising outcomes for various other cancer types such as melanoma, lung cancer, and hematological malignancies in preclinical evaluation (4–6). Despite the promising therapeutic effects of CDK4/6i, many patients eventually develop resistance, which presents a considerable challenge to effective clinical management and long-term survival (7). Accumulating studies, including ourselves, have illustrated mechanisms of resistance to CDK4/6 inhibitors, encompassing alterations in the CDK4/6 pathway (8), activation of compensatory signaling pathways like PI3K/Akt, MAPK/ERK, MITF, and STAT3 pathways (9–12), as well as genetic mutations (13,14). However, CDK4/6i resistance remains a critical clinical challenge in the treatment of breast cancer patients.

Cytokines are soluble proteins that facilitate communication between cells and play vital roles in the immune system and inflammation(15). Numerous studies have implicated cytokines in mediating drug resistance in various types of cancers (16). The platelet-derived growth factors (PDGF) belong to a cytokine family that regulates cell proliferation, differentiation, migration, and angiogenesis. This family comprises four distinct polypeptide chains (PDGF-A, -B, -C, and -D), which form various homodimers or heterodimer isoforms, including PDGF-AA, -AB, -BB, -CC, and -DD (17). PDGF-BB is a key member that primarily binds to its receptor PDGFR-β, a receptor tyrosine kinase (RTK), initiating the formation of dimeric receptor complexes and activating multiple downstream signaling pathways, including PI3K/Akt, MAPK/ERK, and JAK/STAT (18). Recently, PDGF-BB has been reported to be up-regulated in various cancers, promoting tumor growth, angiogenesis,

Author Manuscript Author Manuscript Author Manuscript Author Manuscript

and drug resistance in high-grade glioma, breast cancer, lung adenocarcinoma, and hematological diseases (19–21). Targeting the PDGF/PDGFR signaling pathway has shown excellent clinical therapeutic efficacy and significantly improved patient survival (22). The FDA has approved several potent PDGFR inhibitors for cancer treatment, including sunitinib (23). Despite extensive studies on the role of PDGF-BB in tumors, the intricate regulatory mechanisms governing its expression in cancer remain elusive.

Runt-related transcription factor (RUNX) proteins are members of a transcription factor family that plays critical roles in regulating cell proliferation, apoptosis, differentiation, and lineage determination (24). There are three members of the RUNX family in mammals: RUNX1, RUNX2, and RUNX3, which exhibit distinct tissue-specific expression patterns and biological functions (25). All three RUNX proteins share a highly conserved DNA-binding domain (known as Runt domain), which mediates the interaction with the core-binding factor subunit-β (CBFβ) and facilitates binding to consensus DNA elements (26). It was reported that the RUNX1 is involved in cancer progression, angiogenesis, and chemoresistance (27). Elevated expression of RUNX1 has been found in gastric cancer and hepatocellular carcinoma (28), and RUNX1 is also reported to promote the development of ovarian and skin cancer (29,30). An intriguing intervention in targeting RUNX1 is the identification of Ro5-3335, a potent inhibitor of RUNX1 via interfering RUNX1-CBFβ interaction (31). Numerous studies have shown that RUNX1 activity is regulated by posttranslational modifications (PTMs), including phosphorylation, acetylation, methylation, and ubiquitination (32). The phosphorylation of RUNX1 at S249 and S266 by ERK disrupts its interaction with the transcriptional corepressor SIN3A, leading to enhanced transcriptional activity of RUNX1 (33). RUXN1 is an unstable protein that is subjected to proteolytic degradation via the ubiquitin-proteasome pathway(34). However, the mechanisms governing RUNX1's regulatory framework and its role in physiological responses to drug treatments and drug resistance remain largely unknown.

O-GlcNAcylation is a distinct post-translational modification in which a single N-acetylglucosamine (GlcNAc) sugar moiety is attached to serine or threonine residues of target proteins via a process catalyzed by O-GlcNAc transferase (OGT) or removed by O-GlcNAase (OGA) (35). Dysregulation of O-GlcNAcylation has been implicated in numerous diseases, including cancer, diabetes, neurodegenerative disorders, and cardiovascular diseases(36,37). Yet, the involvement of O-GlcNAc signaling in modulating chemoresistance remains unclear.

In this study, we employed cell coculture, cytokine array, and quantitative high-throughput combinatorial screening (qHTCS) to identify potential cytokines capable of regulating palbociclib resistance. Through these analyses, we found that PDGF-BB is significantly up-regulated in palbociclib-resistant cells and contributes to palbociclib resistance by activating the Akt pathway and suppressing palbociclib-induced senescence. Detailed mechanistic analyses revealed RUNX1 as a new transcription factor that transactivated PDGF-BB in palbociclib-resistant breast cancer cells. Inhibition of RUNX1-PDGF-BB axis by siRNA, neutralizing antibody, and inhibitors (sunitinib and Ro5-3335) re-sensitized resistant cells to palbociclib both *in vitro* and *in vivo*. Strikingly, we discovered for the first time that RUNX1 is O-GlcNAcylated at Serine 252 (S252) by OGT. This O-GlcNAcylation

Author Manuscript Author Manuscript Author Manuscript Author Manuscript

stabilizes RUNX1 protein by blocking its ubiquitination in resistant cells, thus conferring resistance to palbociclib. This novel O-GlcNAcylation of RUNX1-mediated activation of PDGF-BB in resistant cells was further validated in tumor samples from breast cancer patients who received CDK4/6 inhibitor treatment, as well as in PDX models derived from palbociclib sensitive and resistant patients. Together, our findings elucidate a novel mechanism regulating the activation of RUNX1 via O-GlcNAcylation and a previously unappreciated RUNX1-PDGF-BB axis contributing to palbociclib resistance. These results provide clinical evidence to support the development of novel anti-RUNX1-PDGF-BB axis therapeutic approaches to treat CDK4/6i-resistant breast cancer patients by re-purposing FDA-approved PDGFR inhibitor sunitinib.

MATERIALS AND METHODS

Cell culture

The human breast cancer cell lines MCF-7 (RRID:CVCL_0031) and T-47D (RRID: CVCL_0553) were obtained from ATCC and maintained in DMEM medium (Cytiva) supplemented with 10% FBS (Cytiva) at 37°C with 5% CO2. The palbociclib-resistant cell lines MCF-7 PR and T-47D PR were developed by gradually exposing them to increasing concentrations of palbociclib (S1579, Selleckchem) over 6 months. Only early-passage (<10 passages) resistant cells were utilized for this study.

Antibodies, plasmids and chemicals

The antibodies against phospho-Rb (Ser 807/811) (Cell Signaling Technology Cat# 8516, RRID:AB_11178658), total-Rb (Cell Signaling Technology Cat# 9309, RRID:AB_823629), phosphor-Akt (Ser473) (Cell Signaling Technology Cat# 4060, RRID:AB_2315049), total-Akt (Cell Signaling Technology Cat# 9272, RRID:AB_329827), p21 (Cell Signaling Technology Cat# 2947, RRID:AB_823586), GAPDH (Cell Signaling Technology Cat# 2118, RRID:AB_561053), β-Actin (Cell Signaling Technology Cat# 3700, RRID:AB_2242334), PARP (Cell Signaling Technology Cat# 9532, RRID:AB_659884), OGT (Cell Signaling Technology Cat# 24083, RRID:AB_2716710), His-tag (Cell Signaling Technology Cat# 12698, RRID:AB_2744546), FLAG-tag (Cell Signaling Technology Cat# 14793, RRID:AB_2572291), Myc-tag (Cell Signaling Technology Cat# 2276, RRID:AB_331783), HA-tag (Cell Signaling Technology Cat# 3724, RRID:AB_1549585), Cyclin D1 (Cell Signaling Technology Cat# 55506, RRID:AB_2827374), RUNX1 (Cell Signaling Technology Cat# 4336, RRID:AB_10859035) were all from Cell signaling technology; the antibody against PDGFB (Santa Cruz Biotechnology Cat# sc-365805, RRID:AB_10848458) was from Santa Cruz; the antibodies against O-GlcNAc (RL2) (Abcam Cat# ab2739, RRID:AB_303264) and RUNX1 (Abcam Cat #ab240639) were from Abcam. Plasmid expressing HA-RUNX1 RRID:Addgene_181980 was from Addgene; FLAG-STUB1 was from Sino Biological (#HG12496-NF); Myc-tagged OGT was a kind gift from Georgetown University Dr. Huadong Pei lab. RUNX1 mutations were generated using KOD Hot Start DNA polymerase (71086, Sigma-Aldrich), according to the manufacturer's instructions. For generating the stable RUNX1 knock-down cells, two independent shRNAs for RUNX1 were cloned to pLKO.1 vector. The relevant targeting sequences were as follows: shRUNX1–1, CGTAATGACTTATTGTGGATA; shRUNX1–2,

Author Manuscript Author Manuscript Author Manuscript Author Manuscript

GCCTTGAAATACCTGTTTCTT. The chemical AG1296 (#S8024), tricirbine (#S1117) was purchased from Selleckchem.

Cytokine array

Cytokine arrays were conducted in the cell culture medium of MCF-7 WT & MCF-7 PR cells by using the Human Cytokine Antibody Array Kit (Abcam, #ab193656) according to the manufacturer's protocol. Image analysis was performed to quantify the intensity levels using ImageJ software.

siRNA transfections and PCR assay

The following sequences are siRNA duplexes used in this study: si-RUNX1–1, CAGAGUCAGAUGCAGGAUA; si-RUNX1–2, GUUUGUCGGUCGAAGUGGA; si-PDGFB-1, GCAAGCACCGGAAAUUCAA; si-PDGFB-2, GAAAUUCAAGCACACGCAU; siOGT-1, GAUUAAGCCUGUUGAAGUC; siOGT-2, GCUUGCAAUUCAUCACUUU. All transfections were performed using Lipofectamine RNAi MAX (Invitrogen) according to the manufacturer's instructions. Cells were harvested for analysis 48 hrs after siRNA transfection. Total RNA was extracted using the Quick-RNA Purification Kit (Zymo Research), and cDNA was synthesized using the iScript cDNA Synthesis Kit (BIO-RAD). Gene expression was subsequently determined by real-time PCR. All primers are listed in the Supplementary Table 1.

RNA-seq analysis

Total RNA from MCF-7 PR cells transfected with either control or PDGFB siRNA was extracted and processed into cDNA libraries using the Illumina TruSeq Stranded mRNA Sample Preparation Kit (RS-122–2103, Illumina). Gene-set enrichment analysis (GSEA) was conducted using the GSEA software and Hallmark gene signatures as recommended. RNA-Seq data was listed in Supplementary Table 2 and has been deposited into the GEO database with the accession code GSE 264264. RNA-seq data (MCF-7 WT cells and MCF-7 PR cells) analyzed in Figure3A were shown in our previously study with the accession code GSE 234514.

Chromatin immunoprecipitation and qPCR

MCF-7 PR cells were harvested and subjected to chromatin immunoprecipitation using the SimpleChIP Enzymatic Chromatin IP kit (#9003, Cell Signaling Technology), following the manufacturer's instructions. Briefly, cells were cross-linked with 0.4% paraformaldehyde and rotated for 10 minutes at room temperature before quenching with glycine to a final concentration of 0.2M for 15 minutes. After washing, cells were lysed with ChIP lysis buffer and sonicated for approximately 5 minutes. The sonicated chromatin was then incubated with the RUNX1 antibody and rotated overnight. Subsequently, ChIP-Grade Protein G Magnetic Beads were added and rotated for 2 hours. After washing, the beads were eluted with elution buffer. Reverse cross-linking of ChIPed-DNA was performed overnight at 55°C with the addition of 0.3M NaCl, 20 mg RNase A, and 20 mg Proteinase K. Recovery of ChIPed-DNA was achieved using the QIAquick PCR Purification Kit (#28106, QIAGEN).

Author Manuscript Author Manuscript Author Manuscript Author Manuscript

The concentration of ChIPed-DNA was assessed using the Qubit dsDNA HS Assay Kit (Q32851, Invitrogen) and followed by QPCR with PDGFB promoter region primers.

Enzyme-linked immunosorbent assay (ELISA) and Sulforhodamine B (SRB) assay

The ELISA and SRB assay were performed as we described previously (38).

Senescence-associated β-galactosidase assay

Senescence-associated β-galactosidase staining was performed on MCF-7 PR cells and T-47D PR cells using the Cell Signaling Technology kit (#9860), following the manufacturer's instructions.

Co-immunoprecipitation

Co-immunoprecipitation (Co-IP) experiments were conducted by lysing cells with Co-IP buffer containing 20 mM Tris–HCl (pH 8.0), 100 mM NaCl, 1 mM EDTA, 0.5% NP-40, 10 mM NaF, and Protease inhibitor (A32965, ThemoFisher Scientific) on ice for 30 minutes, followed by sonication (10 seconds, three times). After centrifugation, the supernatant was collected and incubated with HA or His beads at 4°C overnight. The beads were then washed three times and analyzed by Western blotting for the indicated proteins.

Mass spectrometry

HEK293T cells were transfected with Myc-OGT and HA-RUNX1 for 48 hours, then cells were harvested for immunoprecipitation (IP). Eluted proteins after immunoprecipitation were resolved by SDS-PAGE followed by Coomassie blue staining. Gel bands were destained and subjected to in-gel digestion with trypsin/LysC. The digests were extracted, cleaned up, and analyzed by nanoUPLC-MS/MS (i.e., nanoAcquity UPLC coupled with an Orbitra Lumos mass spectrometer) in two different mass specs. Modes (i.e., EThcD and HCDpdEThcD) as described previously (39). The resulting data files were analyzed with the software Proteome Discover (v2.40) (Thermo Fisher Scientific) by searching against the customized human RUNX1 protein database. Manual confirmation was performed for the O-GlcNAc sites identified. Mass spectrometry data files were deposited to ProteomeXchange (with identifier PXD049409).

Animal experiments

Six-week-old female BALB/c athymic nude mice were purchased from Jackson Laboratory. A total of 5×10^6 cells were subcutaneously injected into the dorsal flank of each mouse. When the tumor volume reached approximately 100 mm^3, all mice were randomly assigned to the specified experimental groups. Palbociclib was administered intraperitoneally at a dose of 25 mg/kg or 10mg/kg every 2 days for 3 consecutive weeks. RUNX1 inhibitor Ro5-3335 was administered intraperitoneally at a dose of 10 mg/kg every 2 days for 3 consecutive weeks. Saline was used as the control. Relative tumor volumes were measured using calipers to determine the tumor's length (L) and width (W). Measurements are taken while gently restraining the mice to ensure accuracy and minimize stress. The tumor volume is calculated using the formula: $V = (L \times W^2)/2$. Measurements are typically performed every 2–3 days to monitor tumor growth. Mouse organs (heart, lung, liver and kidney)

Author Manuscript Author Manuscript Author Manuscript Author Manuscript

were collected and fixed in 10% formalin, then embedded in paraffin and cut into 4-μm sections for hematoxylin and eosin (H&E) staining. All procedures complied with the National Institutes of Health regulations for the care and use of experimental animals and were approved by the Institutional Animal Care and Use Committee at George Washington University (IACUC Permit No. A2023–013), ensuring humane endpoints if tumors exceeded size limits or caused distress to the animals.

Identification and analysis of RUNX1-PDGFB signature geneset in the NeoPalAna trial

The RUNX1-PDGFB signature geneset was created by overlapping proteins that interact with RUNX1 and genes that are known to be associated with PDGFB function using PathwayNet (40). The overlapping genes of these two groups were selected and named as RUNX1-PDGFB signature geneset (Supplementary Table 2). This geneset was then used to examine the microarray gene expression data obtained from the tumor biopsies in the NeoPalAna trial. Log_2-normalized expression data from baseline samples were used for the analysis. Gene Set Enrichment Analysis (GSEA) software was used to calculate enrichment scores.

PDX-derived organoids

PDX organoids were generated and cultured as previously described (41). Briefly, single cells prepared from PDX tumors were suspended in 50% to 70% growth factor reduced matrigel (#35623, Corning) in breast organoid media modified with 10% Noggin/Rpondin1 conditioned media and 5uM Y-27632 (S1049, Selleckchem). Cultures were fed 2–3 times per week and passed every 7 to 10 days. Organoids were then digested using 1 U/mL dispase (#07923, STEMCELL Technologies) and plated in 96-well or 384-well plates for 2–4 days, then cells were exposed to the drug(s) for 5 days for IC50 and combination assays. This study was approved by Washington University in St. Louis (WUSTL) Human Research Protection Office (HRPO) by following the Declaration of Helsinki and Good Clinical Practice guidelines (IRB Permit No. 201803010). The study was also approved by the Institutional Animal Care and Use Committee at WUSTL (IACUC Permit No. 24–0073), ensuring humane endpoints if tumors exceeded size limits or caused distress to the animals.

Ex vivo drug combination testing on WHIM81 organoids

Organoid cells derived from palbociclib-resistant PDX WHIM81 were plated in matrigel as described above. DMSO or increasing doses of palbociclib and Ro5-3335 (E1245, Selleckchem) or sunitinib (S7781, Selleckchem) were added and incubated for 5 days, and the inhibition of organoid growth was quantified using a CellTiter-Glo 3D cell viability assay (G9683, Promega). Cells growth reading values were normalized to that of the DMSO vehicle. IC50 values were calculated using the 4-parameter, non-linear regression function in GraphPad Prism 5.0 for Windows. Each experiment was repeated three times.

Statistical analysis

Statistical analysis, including unpaired *t*-test and One-way ANOVA as specified in the figure legends, is conducted using GraphPad Prism 9.5.0 software (RRID:SCR_002798). The schematic illustration was created using BioRender (RRID:SCR_018361). Data are

Author Manuscript Author Manuscript Author Manuscript Author Manuscript

presented as mean ± SD or mean ± SEM. Significance is considered when $*P \leq 0.05$ and is indicated in the text as follows: $*P \leq 0.05$, $**P \leq 0.01$, $***P \leq 0.001$, $****P \leq 0.0001$. "NS" indicates no significant difference.

Data availability

The RNA-seq data generated in this study are publicly available in Gene Expression Omnibus (GEO) at GSE264264, and within the supplementary data files. The Mass spectrometry data generated in this study are publicly available in ProteomeXchange via the PRIDE partner repository with the accession number PXD049409, and within the supplementary data files. The RNA-seq data analyzed in this study were obtained from GEO at GSE234514. The DNA microarray data analyzed in this study were obtained from GEO at GSE93204. The TCGA dataset analyzed in this study were obtained from TIMER2.0 (http://timer.cistrome.org/). All other raw data generated in this study are available upon reasonable request from the corresponding author.

RESULTS

Identification of PDGF-BB as a key factor that regulates palbociclib-resistance in breast cancer cells

To investigate whether and how cytokines regulate CDK4/6i-resistance in breast cancer cells, we developed an *in vitro* co-culture system to determine the interaction between palbociclib-resistant (PR) cells (MCF-7 PR and T-47D PR) and their wild-type (WT) counterparts (MCF-7 WT and T-47D WT), which have been described previously (42) and shown in Supp Figure 1A–1B. The PR cells also exhibited resistance to other two CDK4/6i, ribociclib and abemacicilib (Supp Figure 1C–1F). We first labeled MCF-7 WT and MCF-7 PR cells with GFP and RFP, respectively, to facilitate monitoring the growth of each cell line. When cells grew in monoculture with palbociclib treatment, the proliferation of MCF-7 WT cells was significantly suppressed from day 2 to day 8, whereas the growth of MCF-7 PR cells was barely affected (Figure 1A). In contrast, when co-cultured with MCF-7 PR cells, MCF-7 WT cells exhibited sustained growth in response to palbociclib treatment, whereas MCF-7 PR cells displayed a similar growth pattern as in monoculture with palbociclib from day 2 to day 8 (Figure 1A and Supp Figure 1G–1H). Furthermore, we collected conditioned medium (CM) from MCF-7 PR and T-47D PR cells to culture MCF-7 WT and T-47D WT cells respectively. MCF-7 WT and T-47D WT cells cultured in the CM from MCF-7 PR and T-47D PR cells showed remarkably increased resistance to palbociclib compared to cells cultured in the CM from sensitive cells. (Figure 1B and Supp Figure 1I). Collectively, these data strongly indicated that resistant cells may secrete factors that promote palbociclib-resistance of sensitive cells.

As cytokines play crucial roles in regulating cell communication, signaling pathways, and drug resistance (43,44), we aimed to identify specific cytokines in the conditioned medium from resistant cells that mediate palbociclib-resistance of sensitive cells using the cytokine array. The cytokine array revealed 14 cytokines in CM from MCF-7 PR cells and 15 cytokines in CM from T-47D PR cells that were significantly elevated compared to CM from MCF-7 WT and T-47D WT cells respectively (Figure 1C–1D and Supp Figure 1J–1L).

Author Manuscript Author Manuscript Author Manuscript Author Manuscript

We then compared elevated cytokines identified in MCF-7 PR CM with those identified in T-47D PR CM, and found six cytokines: PDGF-BB, AREG, IGFBP6, OPG, sgp130, and STNFRI, were increased in CM of both resistant cell lines (Figure 1E). qPCR analysis confirmed that all these six cytokine genes were up-regulated in resistant cells and PDGF-BB was the most highly expressed gene in both MCF-7 PR and T-47D PR cells compared to their sensitive counterparts (Figure 1F–1G). Consistently, the total level of PDGF-BB protein in resistant cells or secreted PDGF-BB in the medium of resistant cells exhibited a notable elevation compared to their sensitive cells (Supp Figure 1M–1N). Since the PDGF family consists of various homodimer and heterodimer isoforms (20), we examined the expression of these isoforms and found that PDGF-BB but not the others was significantly upregulated in the resistant cells compared to sensitive cells (Supp Figure 1O–1P).

We next investigated the role of PDGF-BB in regulating palbociclib resistance in breast cancer cells. Strikingly, treatment of MCF-7 PR or T-47D PR cells with a PDGF-BB neutralizing antibody restored the sensitivity of cells to palbociclib (Figure 1H and Supp Figure 1Q). Consistently, the addition of recombinant PDGF-BB proteins to the culture medium of sensitive MCF-7 WT or T-47D WT cells induced resistance to palbociclib (Figure 1I and Supp Figure 1R). Additionally, we observed a strong synergy effect between palbociclib and sunitinib (FDA-approved tyrosine kinase receptor inhibitor, which can highly inhibit PDGFR) in resistant cells (Figure 1J and Supp Figure 1S–1T). We found that pre-treatment of cells with the PDGF-BB receptor-specific inhibitor AG1296 also prevented recombinant PDGF-BB from inducing resistance to palbociclib in MCF-7 WT cells (Supp Figure 1U). Accordingly, repression of PDGF-BB by two independent siRNAs re-sensitized both resistant cells to palbociclib (Figure 1K and Supp Figure 1V). Collectively, these results indicated that PDGF-BB is a critical factor in promoting palbociclib-resistance in breast cancer cells.

Inhibition of PDGF-BB overcomes palbociclib-resistance by targeting Akt and inducing the senescence

Previous studies reported that PDGF-BB plays a critical role in regulating intracellular signaling, including PI3K/Akt, MAPK/ERK, and JAK/STAT pathways, which are pivotal in regulating tumorigenesis, cell survival, and drug resistance (20,45–47). We next explored the molecular mechanism by which PDGF-BB regulates palbociclib-resistance. In an independent study to identify compounds that could overcome palbociclib-resistance in breast cancer, we performed a quantitative high-throughput combinatorial screening (qHTCS) using the MIPE (Mechanism Interrogation Plate) and NPC (NCATS Pharmaceutical Collection) small molecular compound libraries as previously described (42). From this screen, Akt inhibitor (Akti) tricirbine emerged as one of the top hits capable of restoring sensitivity to palbociclib in MCF-7 PR cells (Figure 2A). Interestingly, we also observed a significant elevation of p-Akt levels in both resistant cell lines compared to their parental counterparts (Supp Figure 2A). To confirm the synergistic effects of tricirbine with palbociclib, MCF-7 PR cells were treated with a combination of tricirbine and palbociclib for 72 hours, and cell viability was measured and calculated using Combenefit as described previously (48). Remarkably, the combined treatment of tricirbine with palbociclib effectively suppressed the growth of MCF-7 PR cells (Figure 2B and Supp Figure 2B).

Author Manuscript Author Manuscript Author Manuscript Author Manuscript

To identify the downstream targets of PDGF-BB in resistant cells, we conducted RNA-seq analysis in MCF-PR cells with PDGF-BB down-regulation by siRNA. Consistently, analysis of gene expression profile from RNA-seq data showed that inhibition of PDGF-BB decreased the enrichment of the PI3K-Akt geneset in MCF-7 PR cells, indicating that PI3K-Akt signaling is a downstream target of PDGF-BB (Figure 2C**, left**). Furthermore, PDGF-BB depletion also reduced the E2F geneset, indicating a cell cycle arrest (Figure 2C**, right**). Consistently, Western blotting showed that inhibition of PDGF-BB significantly reduced the levels of p-Akt, suggesting the repression of the Akt pathway (Figure 2D). Strikingly, pre-treating resistant cells with an Akt agonist SC-79 prevented the restoration of sensitivity to palbociclib by PDGF-BB knockdown in both MCF-7 PR and T-47D PR cells (Figure 2E–2F), suggesting that Akt is a primary target of PDGF-BB in resistant cells.

PDGF-BB inhibition increased the expression levels of p21 and p27 (Figure 2D), which are considered as the biomarkers of senescence (49). We therefore assumed that a combination of PDGF-BB inhibition and palbociclib may induce senescence in resistant cells. Indeed, in PR cells depletion of PDGF-BB in combination with palbociclib further increased p21 levels, and decreased levels of p-Rb and Cyclin D1 compared to treatment with palbociclib alone (Figure 2G–2H), suggesting that the combination of PDGF-BB repression with palbociclib treatment promoted the cell cycle arrest and activated the senescence in PR cells. Suppression of PDGF-BB together with palbociclib did not induce apoptosis as indicated by the absence of cleaved PARP (Figure 2G–2H). Thus, inhibition of PDGF-BB may restore the sensitivity of resistant cells to palbociclib by inducing senescence rather than apoptosis. In agreement with this notion, inhibition of PDGF-BB alone increased the number of cells with positive staining of senescence-associated β-galactosidase (SA-β-Gal), a well-known marker of senescent cells (49), while inhibition of PDGF-BB together with palbociclib further augmented the population of SA-β-Gal positive cells (Figure 2I and Supp Figure 2C). Collectively, these data indicated that inhibition of PDGF-BB overcomes palbociclib-resistance by downregulating the Akt pathway and inducing senescence in resistant breast cancer cells.

RUNX1 is a transcription factor regulating expression of PDGF-BB in palbociclib-resistant cells

Given that the PDGF-BB mRNA level is elevated in palbociclib-resistant cells (Figure 1F), we next explored how PDGF-BB is upregulated transcriptionally in resistant cells. To this end, we identified all transcription factors (TF) that could bind the promoter region of PDGF-BB by using the JASPAR database (50). Comparing the upregulated genes in RNA-seq data from MCF-7 PR cells with these TFs, along with the PDGF-BB transcription-regulated genes obtained from the Pahtwaynet analysis (40), we identified RUNX1 as a potential TF regulating PDGF-BB transcription in resistant cells (Figure 3A). Interestingly, both mRNA and protein levels of RUNX1 were significantly elevated in MCF-7 PR and T-47D PR cells compared to their sensitive counterparts (Figure 3B). To explore whether RUNX1 directly binds to the PDGF-BB promoter region, we performed ChIP-qPCR assay and found that RUNX1 was indeed enriched at the promotor region of PDGF-BB in MCF-7 PR cells (Figure 3C). Furthermore, luciferase report assay demonstrated that RUNX1 could directly transactivate PDGF-BB expression (Figure 3D). To support the notion that RUNX1

Author Manuscript Author Manuscript Author Manuscript Author Manuscript

is a newly identified transcription factor of PDGF-BB, inhibition of RUNX1 by siRNA reduced mRNA and protein levels of PDGF-BB (Figure 3E and Supp Figure 3A), and re-sensitized both resistant cells to palbociclib (Figure 3F and Supp Figure 3B).

To demonstrate that RUNX1 regulates palbociclib-resistance by controlling expression of PDGF-BB, we measured the levels of p-Akt (Ser473), p-Rb, and Cyclin D1 in resistant cells treated with siRNA against RUNX1, followed by the addition of recombinant PDGF-BB protein. Strikingly, treatment with recombinant PDGF-BB protein robustly restored the expression of p-Akt, p-Rb, and CyclinD1 in resistant cells with RUNX1 knockdown, suggesting the activation of Akt and the cell cycle progression (Figure 3G–3H). Additionally, cell viability was moderately restored in resistant cells treated with recombinant PDGF-BB protein compared to cells without PDGF-BB protein treatment (Figure 3I–3J). In line with these findings, the combined treatment of palbociclib with RUNX1 inhibitor (Ro5-3335) (31) demonstrated significant synergistic effects in MCF-7 PR cells *in vitro* and *in vivo* (Figure 3K–3M and Supp Figure 3C). To precisely measure the synergy, we calculated the combination index (CI), which measures the drug interactions (synergism: CI < 1; additive effect: CI = 1; antagonism: CI > 1) (51). The results revealed a strong synergy in resistant cells, but not in sensitive cells (Supp Figure 3D–3E). We next evaluated the toxicity of the combination treatment by monitoring the body weight of all treated mice and conducting H&E staining on multiple organs, including the heart, lung, kidney, and liver. We observed neither weight changes of treated mice, nor systemic toxicity in these examined organs (Supp Figure 3F–3M).

Together, these results suggest that RUNX1 is a previously unappreciated transcription factor that transcriptionally activates PDGF-BB to promote palbociclib resistance in breast cancer.

O-GlcNAcylation of RUNX1 by OGT promotes its protein stability

Our above findings elucidated a novel mechanism regulating the transcription of PDGF-BB via the transcription factor RUNX1 in palbociclib-resistant cells. We next investigated whether and how RUNX1 itself is regulated in resistant cells. Although RUNX1 mRNA level was significantly upregulated in resistant cells (Figure 3B), the protein is highly unstable and prone to ubiquitin-mediated degradation (52). Given that RUNX1 protein is also largely up-regulated in resistant cells (Figure 3B), we hypothesized that there may be PTMs involved in regulating RUNX1 protein stability in resistant cells. Several studies have reported that OGT-mediated O-GlcNAcylation can stabilize the protein by preventing its degradation, thus promoting tumor progression or chemo-resistance (53–55). We therefore speculated that OGT-mediated O-GlcNAcylation may regulate the stability of RUNX1 protein in palbociclib-resistance cells. To support this hypothesis, we confirmed that both mRNA and protein levels of OGT were significantly elevated in resistant cells compared to sensitive cells (Supp Figure 4A–4C). Strikingly, we found that RUNX1 interacted with OGT and was O-GlcNAcylated (Figure 4A), while the O-GlcNAcylation level of RUNX1 was significantly decreased in OGT knockdown (Figure 4B and Supp Figure 4D). Interestingly, RUNX1 protein level was notably reduced in both MCF-7 PR and T-47D PR cells with OGT knockdown (Figure 4C), whereas mRNA expression of RUNX1 was not affected (Figure

Author Manuscript Author Manuscript Author Manuscript Author Manuscript

4D). Moreover, overexpression of OGT notably increased the levels of RUNX1 protein in both sensitive cells (Figure 4E and Supp Figure 4E–4F). Thus, OGT appears to regulate the stability of the RUNX1 protein through post-translational modifications.

To further investigate the mechanism of how O-GlcNAcylation regulates RUNX1 protein stability, we treated MCF-7 PR cells with cycloheximide (CHX) to inhibit protein synthesis following OGT knockdown. The protein level of RUNX1 exhibited an 80% reduction in cells treated with siOGT 4 hours post-CHX treatment compared to an approximate 50% reduction in the control-treated cells (Figure 4F–4G). A similar outcome was also observed in T-47D PR cells (Supp Figure 4G). These findings suggest that OGT-mediated O-GlcNAcylation is involved in maintaining the stability of RUNX1 protein in palbociclib-resistance cells.

We next explored whether RUNX1 O-GlcNAcylation regulates its stability by affecting the ubiquitin-mediated pathway. Remarkably, the ubiquitination of RUNX1 was significantly increased following OGT knockdown, whereas overexpression of OGT notably decreased the ubiquitination level of RUNX1 (Figure 4H–4I), indicating a cross-talk between O-GlcNAcylation and ubiquitination in the regulation of RUNX1 stability. STUB1 is a ubiquitin E3 ligase that interacts with RUNX1, inducing its ubiquitination and subsequent degradation (52). We examined whether OGT promotes RUNX1 stability by affecting RUNX1-STUB1 interaction. Indeed, the depletion of OGT significantly increased the association between STUB1 and RUNX1 (Figure 4J). In contrast, the interaction between STUB1 and RUNX1 gradually decreased with simultaneously increased OGT expression, and the protein level of RUNX1 was also increased by OGT in a dose-dependent manner (Figure 4K). Accordingly, the depletion of OGT sensitized MCF-7 PR cells to palbociclib (Supp Figure 4H). Furthermore, inhibition of O-GlcNAcylation did not affect the interaction between RUNX1 and CBFβ (Supp Figure 4I–4J), the co-binding factor of RUNX1(56). Taken together, these results indicated that in resistant cells, OGT-mediated O-GlcNAcylation of RUNX1 promotes its protein stability by preventing its interaction with E3 ligase STUB1.

O-GlcNAcylation of RUNX1 at Serine 252 is required for its stability and palbociclib-resistance

To further investigate how O-GlcNAcylation regulates the stability of RUNX1, we conducted a mass spectrometry assay to identify the specific O-glycosylation site(s) of RUNX1. The analysis identified seven potential O-GlcNAcylation sites (Ser53, Thr234, Ser239, Thr246, Ser252, Ser331, and Ser362) of RUNX1(localization score: >0.75; Supplementary Table 3). We then introduced alanine mutations to each of these identified O-GlcNAc sites and assessed the O-GlcNAcylation signal of RUNX1. It turned out that the O-GlcNAc level of RUNX1 was significantly reduced in the S252A mutant rather than the other mutants (Figure 5A–5B), suggesting that S252 is the dominant O-GlcNAc site of RUNX1. Sequence comparison analysis showed that RUNX1 S252 is conserved across various species (Figure 5C).

We then explored whether the mutation of RUNX1 at S252 affected its protein stability. The S252A mutant exhibited higher levels of ubiquitination compared to RUNX1 WT (Figure

Author Manuscript Author Manuscript Author Manuscript Author Manuscript

5D). Additionally, in cells with OGT knockdown, WT RUNX1 exhibited a significantly increased level of ubiquitination compared to the control cells, whereas the S252A mutant did not exhibit significant changes (Figure 5D). In contrast, OGT overexpression reduced the ubiquitination level of RUNX1 WT, whereas the S252A mutant exhibited no substantial changes (Figure 5E). Furthermore, protein stability of exogenously expressed RUNX1 S252A was reduced compared to WT RUNX1, in both MCF-7 WT and T-47D WT cells (Figure 5F–5G). Consistently, we observed an increased interaction between the S252A mutant and STUB1 compared to RUNX1 WT (Figure 5H). Together, these findings suggest that the loss of O-GlcNAcylation at S252 of RUNX1 enhances the interaction between STUB1 and RUNX1, consequently promoting the degradation of RUNX1 by STUB1-mediated ubiquitination.

We next investigated how O-GlcNAcylation at S252 of RUNX1 regulates the response to palbociclib in resistant cells. Although depletion of RUNX1 re-sensitized MCF-7 PR cells to palbociclib, reconstitution of RUNX1 WT but not S252A mutant in RUNX1-depleted cells restored the resistance to palbociclib (Figure 5I). Consistently, reconstitution of RUNX1 WT restored the expression of PDGF-BB but not the S252A mutant in RUNX1 depleted-MCF-7 PR cells (Supp Figure 5A–5C). In line with the observations shown in Supp Figure 4F–4G, the interactions between RUNX1 WT or S252A with CBFβ were not affected (Supp Figure 5D). Using xenografted tumor models, we also found that the reintroduction of RUNX1 WT but not S252A mutant in RUNX1 depleted-MCF-7 PR cells restored resistance to palbociclib *in vivo* (Figure 5J). Thus, the O-GlcNAcylation of RUNX1 at S252 plays a pivotal role in regulating its protein stability and resistance to palbociclib in breast cancer cells.

Palbociclib treatment activates the RUNX1-PDGF-BB axis both *in vitro* and *in vivo*

We next investigated the molecular mechanism underlying how breast cancer cells develop resistance to palbociclib during treatment. Considering the observed elevation in RUNX1-PDGF-BB levels is associated with palbociclib resistance, it is highly possible that the RUNX1-PDGF-BB axis is activated in response to palbociclib treatment as a compensatory survival mechanism for breast cancer cells. Indeed, the mRNA and the protein level of RUNX1 and PDGF-BB, as well as the p-Akt level, were increased in a dose-dependent and time-dependent manner upon palbociclib treatment in MCF-7 WT and T-47D WT cells (Figure 6A–6C and Supp Figure 6A–6C). Similarly, the secretion of PDGF-BB was also increased in response to palbociclib treatment (Figure 6D and Supp Figure 6D). In line with these findings, the other two CDK4/6 inhibitors, ribociclib and abemaciclib, also significantly increased the levels of RUNX1, PDGF-BB, and p-Akt in dose- and time-dependent manners in MCF-7 WT cells (Supp Figure 6E–6F). To further investigate whether breast cancer cells exhibit a similar response to palbociclib *in vivo*, we treated MCF-7 WT xenograft tumors with a low dose palbociclib (10mg/kg) for 3 weeks (Figure 6E). Although low-dose palbociclib treatment reduced the MCF-7 WT xenograft tumor volume (Figure 6F) and the decreased p-Rb level of the xenografts, which suggested breast cancer cells' cycle were arrested, we observed a substantial increase in the levels of RUNX1 and PDGF-BB compared with the control group (Figure 6G–6H). Thus, palbociclib treatment can induce the activation of the RUNX1-PDGF-BB axis in tumor cells *in vivo*. Moreover,

Author Manuscript Author Manuscript Author Manuscript Author Manuscript

overexpression of OGT, RUNX1, or OGT and RUNX1 together in MCF-7 WT cells and T-47D WT cells increased the PDGF-BB protein levels (Figure 6I and Supp Figure 6G) and induced resistance to palbociclib (Figure 6J and Supp Figure 6H). These results provide both in *vitro* and in *vivo* evidence that elucidates the process for breast cancer cells to develop RUNX1-PDGF-BB axis-mediated resistance in response to palbociclib treatment.

RUNX1-PDGF-BB axis is activated in response to palbociclib treatment in breast cancer patients

Given that the RUNX1-PDGF-BB axis is induced by palbociclib treatment and is required for palbociclib resistance in breast cancer cells, we next conducted studies to examine whether this axis is activated in patients undergoing CDK4/6i treatment in clinical studies. We first analyzed the gene expression data obtained from 120 tumor biopsies collected at 4 different timepoints from 50 patients with phase II/III estrogen receptor-positive breast cancer enrolled in the NeopalAna trial (57) (Figure 7A). The cytokine geneset was significantly enriched in patients after palbociclib treatment (16–20 weeks after palbociclib administration) (surgery timepoint) compared to the early timepoints (C1D1 and C1D15) (Figure 7B). To further examine the involvement of the RUNX1-PDGF-BB axis in response to palbociclib in breast cancer, we created a RUNX1-PDGF-BB signature gene set by overlapping proteins known to interact with RUNX1 and genes associated with PDGF-BB function, as determined by PathwayNet analysis. Remarkably, we observed significant enrichment of the RUNX1-PDGF-BB signature geneset at the surgery timepoint compared to the C1D15 timepoint (Figure 7C). Moreover, the RUNX1-PDGF-BB signature geneset was also enriched at the surgery and C1D15 timepoints in palbociclib-resistant patients compared to sensitive patients, while no significant difference was observed at the C1D1 stage (Supp Figure 7A).

To further confirm the significance of the elevated RUNX1-PDGF-BB axis in driving palbociclib resistance in breast cancer, we assessed RUNX1-PDGF-BB expression in a cohort of patient-derived xenograft (PDX) lines, which comprised 7 palbociclib-sensitive lines and 7 palbociclib-resistant lines. Remarkably, the expression levels of RUNX1, PDGF-BB, OGT, and O-GlcNAc were notably elevated in the majority of palbociclib-resistant PDX lines when compared to the sensitive PDX lines (Figure 7D–7F).

Breast cancer organoids effectively capture the heterogeneity of the disease, making them widely utilized as clinical models for drug discovery and precision oncology (41,58). To explore the potential application of the anti-RUNX1-PDGF-BB strategy for the treatment of resistant patients, we established a palbociclib-resistant organoid derived from the palbociclib-resistant PDX WHIM81 to evaluate the efficacy of combined treatment of palbociclib with RUNX1 inhibitor (Ro5-3335) or PDGFR inhibitor (sunitinib). In line with the findings shown in Figure 3K, palbociclib exhibited great synergy with Ro5-3335 in this palbociclib-resistant organoid model (Figure 7G and Supp Figure 7B). Moreover, sunitinib demonstrated strong synergy with palbociclib in this palbociclib-resistant organoid (Figure 7H and Supp Figure 7C). We also analyzed the expression levels of RUNX1 and PDGF-BB using data from the TCGA database and found that PDGF-BB expression levels exhibited a significantly positive correlation with RUNX1 in breast cancer patients (Supp

Author Manuscript Author Manuscript Author Manuscript Author Manuscript

Figure 7D), supporting our discovery that RUNX1 regulates transcription of PDGF-BB. Collectively, these clinical data strongly suggest that palbociclib treatment activates the RUNX1-PDGF-BB axis, the elevated RUNX1-PDGF-BB axis is seen in resistant PDX lines, and inhibition of RUNX1-PDGF-BB by their inhibitors overcomes palbociclib-resistance in resistant organoid model.

DISCUSSION

In this study, we have unveiled a novel RUNX1-PDGF-BB axis that is activated in palbociclib-resistant cells and plays a crucial role in regulating resistance to CDK4/6i in breast cancer cells. We found that palbociclib-resistant cells secret PDGF-BB which promotes the growth of palbociclib-sensitive cells. Inhibition of PDGF-BB overcomes palbociclib resistance by suppressing the PI3K/Akt pathway and inducing senescence in palbociclib-resistant cells. Significantly, we identified RUNX1 as a transcription factor of PDGF-BB, which is activated in resistant cells. For the first time, we found that RUNX1 is O-GlcNAcylated by OGT at the S252 site, preventing RUNX1 degradation, thus resulting in PDGF-BB-mediated resistance to palbociclib in breast cancer cells (Figure 7I). Inhibition of RUNX1-PDGF-BB was able to restore the sensitivity of resistant breast cancer cells to palbociclib in vitro and in vivo. Our study also provides strong clinical evidence supporting the notion that the activated RUNX1-PDGF-BB axis contributes to resistance to palbociclib.

The role of cytokines in the regulation of tumor progression has gained significant attention in the cancer research field recently. For example, activated IL-11/Jak2 signaling leads to platinum resistance in ovarian cancer (59), and the IL-6/STA3 pathway contributes to palbociclib resistance in breast cancer (10). Several cytokines, including IL-2 and IFN-α, have shown modest clinical benefits and have been approved by the FDA for the treatment of certain malignant diseases (60,61). PDGF-BB, as one of the most important members in the PDGF family, is elevated in numerous cancers and correlated with increased proliferation, invasion, and metastasis (20). Upregulation of PDGF-BB was observed in approximately 70% of the NSCLS patient tissue (62). Besides, inhibition of PDGF-BB/PDGFRβ signaling reduces vessel functionality and tumor growth in breast carcinogenesis (63). Our study demonstrated that suppression of PDGF-BB overcomes palbociclib resistance by downregulating the Akt pathway and inducing senescence in palbociclib-resistant breast cancer cells. Previous studies have shown that activation of the Akt pathway suppresses senescence and promotes tumorigenesis (64), while inhibition of PI3K/Akt signaling directly induced premature senescence and increased expression of p21 (65). In line with these findings, our data discovered a new mechanism by which PDGF-BB regulates senescence and Akt activation in palbociclib-resistant cells.

RUNX1, also known as acute myeloid leukemia gene 1 (AML1), is renowned for its involvement in the t(8;21) translocation observed in cancer patients with AML (66). To date, emerging studies have highlighted the role of RUNX1 in regulating drug resistance in cancer. Specifically, RUNX1 has been identified as the transcription factor of HDAC2, which is essential for 5-FU chemoresistance (67). Moreover, RUNX1 coordinates with FUBP1 to activate the oncogene c-KIT, resulting in increased resistance to the imatinib mesylate in AML (68). Our results demonstrate that RUNX1 is upregulated in the

Author Manuscript Author Manuscript Author Manuscript Author Manuscript

palbociclib-resistant cells and acts as a new transcription factor of PDGF-BB to transactivate PDGF-BB expression in resistant cells.

RUNX1 activity is modulated by multiple post-translational modifications (PTMs), including phosphorylation, acetylation, methylation, and ubiquitination, which can alternate its transcriptional activity via affecting its protein stability or interaction with other proteins. For example, RUNX1 is acetylated at K24 and K43 by p300, therefore augmenting the RUNX1 DNA-binding activity and transcriptional activity (69). RUNX1 is an unstable protein that is subjected to proteolytic degradation mediated by the ubiquitin-proteasome pathway (70). Our results indicate that the RUNX1 protein is upregulated in palbociclib-resistant cells via a previously unappreciated pathway O-GlcNAcylation at S252. Cross-talk between ubiquitination and O-GlcNAcylation has been reported. For example, O-GlcNAcylation of SIRT7 at S136 can inhibit its ubiquitination, thereby stabilizing SIRT7 protein expression and promoting pancreatic cancer progression (53). We still do not know the detailed mechanism of how O-GlcNAcylation of RUNX1 prevents its ubiquitination-mediated by E3 ligase STUB1. One possible explanation is that O-GlcNAcylation may induce a conformational change in RUNX1, blocking the interaction between RUNX1 and STUB1. Further structural analysis is required to elucidate how O-GlcNAcylation affects its conformation, and such studies could provide valuable insights into the mechanisms underlying RUNX1-mediated palbociclib resistance in breast cancer cells.

Our studies using clinical samples from the NeoPalAna trial unveiled that the administration of palbociclib results in an enrichment of the cytokine geneset and the RUNX1-PDGF-BB geneset from breast cancer patients (shown in Figure 7), which strongly support our observation that RUNX1-PDGF-BB axis is activated by CDK4/6i in a time and dose-dependent manner (shown in Figure 6). Thus, our clinical studies strongly suggest that the activation of the RUNX1-PDGF-BB axis triggered by CDK4/6i may function as a survival mechanism utilized by cancer cells in response to CDK4/6 inhibition and that the activated RUNX1-PDGF-BB axis is a novel pathway causing resistance to CDK4/6i in breast cancer. Inhibition of RUNX1 by Ro5-3335, or blocking PDGF-BB signaling transduction via tyrosine kinases receptor inhibitor sunitinib (FDA-approved drug), both displayed a good synergy with palbociclib in the palbociclib-resistant PDX organoid model WHIM81 (Figure 7G–7H). Our studies provide clinical evidence to support a potential therapeutic strategy to treat resistance to CDK4/6i in breast cancer patients by repurposing FDA-approved drugs.

In this study, we employed a range of palbociclib concentrations *in vitro* to investigate mechanisms underlying CDK4/6i resistance and to evaluate potential therapeutic combinations to overcome it. The drug concentrations were selected based on IC50 values obtained from dose-response experiments and previously published studies (71–73). We acknowledge that the concentrations used in our in vitro experiments exceed the therapeutic doses typically administered in clinical settings and may not fully replicate the pharmacodynamics observed in patients. However, it is important to note that drug concentrations validated in cellular studies sometimes differ from those used in vivo due to variations in cellular metabolism, bioavailability, and the microenvironment between the two systems. As a proof-of-concept study, our primary objective was to characterize a novel mechanism of CDK4/6i resistance and provide preclinical evidence to support future

Author Manuscript Author Manuscript Author Manuscript Author Manuscript

clinical applications. Moving forward, studies incorporating physiologically relevant doses and oral gavage administration of palbociclib in preclinical animal models will enhance the translational relevance of our findings and offer a more accurate assessment of the therapeutic efficacy of these novel drug combinations in clinical settings.

Supplementary Material

Refer to Web version on PubMed Central for supplementary material.

ACKNOWLEDGMENTS

This work was partially supported by funding from the National Institutes of Health (CA247684, CA258357, and CA184717 to W.Z.), and a grant from the McCormick Genomic and Proteomic Center. High-throughput drug screening assay in this research was supported by the Intramural Research Program of the NIH, National Cancer Institute and the National Center for Advancing Translational Sciences. Mass spectrometry analysis conducted in this study was partially supported by NCI-P30CA051008.

REFERENCE

1. Portman N, Alexandrou S, Carson E, Wang S, Lim E, Caldon CE. Overcoming CDK4/6 inhibitor resistance in ER-positive breast cancer. Endocr Relat Cancer 2019;26:R15–R30 [PubMed: 30389903]
2. Goel S, DeCristo MJ, McAllister SS, Zhao JJ. CDK4/6 Inhibition in Cancer: Beyond Cell Cycle Arrest. Trends Cell Biol 2018;28:911–25 [PubMed: 30061045]
3. Finn RS, Aleshin A, Slamon DJ. Targeting the cyclin-dependent kinases (CDK) 4/6 in estrogen receptor-positive breast cancers. Breast Cancer Res 2016;18:17 [PubMed: 26857361]
4. Sheppard KE, McArthur GA. The cell-cycle regulator CDK4: an emerging therapeutic target in melanoma. Clin Cancer Res 2013;19:5320–8 [PubMed: 24089445]
5. Bai X, Guo ZQ, Zhang YP, Fan ZZ, Liu LJ, Liu L, et al. CDK4/6 inhibition triggers ICAM1-driven immune response and sensitizes LKB1 mutant lung cancer to immunotherapy. Nat Commun 2023;14:1247 [PubMed: 36871040]
6. Bride KL, Hu H, Tikhonova A, Fuller TJ, Vincent TL, Shraim R, et al. Rational drug combinations with CDK4/6 inhibitors in acute lymphoblastic leukemia. Haematologica 2022;107:1746–57 [PubMed: 34937317]
7. Xu XQ, Pan XH, Wang TT, Wang J, Yang B, He QJ, et al. Intrinsic and acquired resistance to CDK4/6 inhibitors and potential overcoming strategies. Acta Pharmacol Sin 2021;42:171–8 [PubMed: 32504067]
8. Yang C, Li Z, Bhatt T, Dickler M, Giri D, Scaltriti M, et al. Acquired CDK6 amplification promotes breast cancer resistance to CDK4/6 inhibitors and loss of ER signaling and dependence. Oncogene 2017;36:2255–64 [PubMed: 27748766]
9. Alves CL, Ehmsen S, Terp MG, Portman N, Tuttolomondo M, Gammelgaard OL, et al. Co-targeting CDK4/6 and AKT with endocrine therapy prevents progression in CDK4/6 inhibitor and endocrine therapy-resistant breast cancer. Nat Commun 2021;12:5112 [PubMed: 34433817]
10. Kettner NM, Vijayaraghavan S, Durak MG, Bui T, Kohansal M, Ha MJ, et al. Combined Inhibition of STAT3 and DNA Repair in Palbociclib-Resistant ER-Positive Breast Cancer. Clin Cancer Res 2019;25:3996–4013 [PubMed: 30867218]
11. Adamia S, Bhatt S, Wen K, Chyra Z, Fell GG, Tai YT, et al. Combination therapy targeting Erk1/2 and CDK4/6i in relapsed refractory multiple myeloma. Leukemia 2022;36:1088–101 [PubMed: 35082402]
12. Zhang Y, Zhou S, Kai Y, Zhang YQ, Peng C, Li Z, et al. O-GlcNAcylation of MITF regulates its activity and CDK4/6 inhibitor resistance in breast cancer. Nat Commun 2024;15:5597 [PubMed: 38961064]

Author Manuscript Author Manuscript Author Manuscript Author Manuscript

13. Pandey K, An HJ, Kim SK, Lee SA, Kim S, Lim SM, et al. Molecular mechanisms of resistance to CDK4/6 inhibitors in breast cancer: A review. Int J Cancer 2019;145:1179–88 [PubMed: 30478914]
14. Condorelli R, Spring L, O'Shaughnessy J, Lacroix L, Bailleux C, Scott V, et al. Polyclonal RB1 mutations and acquired resistance to CDK 4/6 inhibitors in patients with metastatic breast cancer. Ann Oncol 2018;29:640–5 [PubMed: 29236940]
15. Altan-Bonnet G, Mukherjee R. Cytokine-mediated communication: a quantitative appraisal of immune complexity. Nat Rev Immunol 2019;19:205–17 [PubMed: 30770905]
16. Cavazzoni A, Digiacomo G. Role of Cytokines and Other Soluble Factors in Tumor Development: Rationale for New Therapeutic Strategies. Cells 2023;12
17. Fredriksson L, Li H, Eriksson U. The PDGF family: four gene products form five dimeric isoforms. Cytokine Growth Factor Rev 2004;15:197–204 [PubMed: 15207811]
18. Ouyang L, Zhang K, Chen J, Wang J, Huang H. Roles of platelet-derived growth factor in vascular calcification. J Cell Physiol 2018;233:2804–14 [PubMed: 28467642]
19. Ross JL, Chen Z, Herting CJ, Grabovska Y, Szulzewsky F, Puigdelloses M, et al. Platelet-derived growth factor beta is a potent inflammatory driver in paediatric high-grade glioma. Brain 2021;144:53–69 [PubMed: 33300045]
20. Xiu-Ying H, Yue-Xiang Z, Hui-Si Y, Hong-Zhou Y, Qing-Jie X, Ting-Hua W. PDGFBB facilitates tumorigenesis and malignancy of lung adenocarcinoma associated with PI3K-AKT/MAPK signaling. Sci Rep 2024;14:4191 [PubMed: 38378786]
21. Tchougounova E, Kastemar M, Brasater D, Holland EC, Westermark B, Uhrbom L. Loss of Arf causes tumor progression of PDGFB-induced oligodendroglioma. Oncogene 2007;26:6289–96 [PubMed: 17438529]
22. Homsi J, Daud AI. Spectrum of activity and mechanism of action of VEGF/PDGF inhibitors. Cancer Control 2007;14:285–94 [PubMed: 17615535]
23. Sun Y, Yue L, Xu P, Hu W. An overview of agents and treatments for PDGFRA-mutated gastrointestinal stromal tumors. Front Oncol 2022;12:927587 [PubMed: 36119525]
24. Ito Y, Bae SC, Chuang LS. The RUNX family: developmental regulators in cancer. Nat Rev Cancer 2015;15:81–95 [PubMed: 25592647]
25. Tuo Z, Zhang Y, Wang X, Dai S, Liu K, Xia D, et al. RUNX1 is a promising prognostic biomarker and related to immune infiltrates of cancer-associated fibroblasts in human cancers. BMC Cancer 2022;22:523 [PubMed: 35534796]
26. Tahirov TH, Inoue-Bungo T, Morii H, Fujikawa A, Sasaki M, Kimura K, et al. Structural analyses of DNA recognition by the AML1/Runx-1 Runt domain and its allosteric control by CBFbeta. Cell 2001;104:755–67 [PubMed: 11257229]
27. Li Q, Lai Q, He C, Fang Y, Yan Q, Zhang Y, et al. RUNX1 promotes tumour metastasis by activating the Wnt/beta-catenin signalling pathway and EMT in colorectal cancer. J Exp Clin Cancer Res 2019;38:334 [PubMed: 31370857]
28. Liu C, Xu D, Xue B, Liu B, Li J, Huang J. Upregulation of RUNX1 Suppresses Proliferation and Migration through Repressing VEGFA Expression in Hepatocellular Carcinoma. Pathol Oncol Res 2020;26:1301–11 [PubMed: 31289995]
29. Xiao L, Peng Z, Zhu A, Xue R, Lu R, Mi J, et al. Inhibition of RUNX1 promotes cisplatin-induced apoptosis in ovarian cancer cells. Biochem Pharmacol 2020;180:114116 [PubMed: 32579960]
30. Scheitz CJ, Lee TS, McDermitt DJ, Tumbar T. Defining a tissue stem cell-driven Runx1/Stat3 signalling axis in epithelial cancer. EMBO J 2012;31:4124–39 [PubMed: 23034403]
31. Cunningham L, Finckbeiner S, Hyde RK, Southall N, Marugan J, Yedavalli VR, et al. Identification of benzodiazepine Ro5-3335 as an inhibitor of CBF leukemia through quantitative high throughput screen against RUNX1-CBFbeta interaction. Proc Natl Acad Sci U S A 2012;109:14592–7 [PubMed: 22912405]
32. Wang L, Huang G, Zhao X, Hatlen MA, Vu L, Liu F, et al. Post-translational modifications of Runx1 regulate its activity in the cell. Blood Cells Mol Dis 2009;43:30–4 [PubMed: 19386523]
33. Imai Y, Kurokawa M, Yamaguchi Y, Izutsu K, Nitta E, Mitani K, et al. The corepressor mSin3A regulates phosphorylation-induced activation, intranuclear location, and stability of AML1. Mol Cell Biol 2004;24:1033–43 [PubMed: 14729951]

Author Manuscript Author Manuscript Author Manuscript Author Manuscript

34. Huang G, Shigesada K, Ito K, Wee HJ, Yokomizo T, Ito Y. Dimerization with PEBP2beta protects RUNX1/AML1 from ubiquitin-proteasome-mediated degradation. EMBO J 2001;20:723–33 [PubMed: 11179217]
35. Hart GW, Housley MP, Slawson C. Cycling of O-linked beta-N-acetylglucosamine on nucleocytoplasmic proteins. Nature 2007;446:1017–22 [PubMed: 17460662]
36. Hart GW. Nutrient regulation of signaling and transcription. J Biol Chem 2019;294:2211–31 [PubMed: 30626734]
37. Chatham JC, Zhang J, Wende AR. Role of O-Linked N-Acetylglucosamine Protein Modification in Cellular (Patho)Physiology. Physiol Rev 2021;101:427–93 [PubMed: 32730113]
38. Zhang Y, Li J, Zhou Y, Li Z, Peng C, Pei H, et al. And-1 Coordinates with the FANCM Complex to Regulate Fanconi Anemia Signaling and Cisplatin Resistance. Cancer Res 2022;82:3249–62 [PubMed: 35867033]
39. Wu C, Shi S, Hou C, Luo Y, Byers S, Ma J. Design and Preparation of Novel Nitro-Oxide-Grafted Nanospheres with Enhanced Hydrogen Bonding Interaction for O-GlcNAc Analysis. ACS Appl Mater Interfaces 2022;14:47482–90 [PubMed: 36240223]
40. Park CY, Krishnan A, Zhu Q, Wong AK, Lee YS, Troyanskaya OG. Tissue-aware data integration approach for the inference of pathway interactions in metazoan organisms. Bioinformatics 2015;31:1093–101 [PubMed: 25431329]
41. Sachs N, de Ligt J, Kopper O, Gogola E, Bounova G, Weeber F, et al. A Living Biobank of Breast Cancer Organoids Captures Disease Heterogeneity. Cell 2018;172:373–86 e10 [PubMed: 29224780]
42. Yi Z, et al. . O-GlcNAcylation of MITF regulates its activity and CDK4/6 inhibitor resistance in breast cancer. Nat Commun 2024
43. Setrerrahmane S, Xu H. Tumor-related interleukins: old validated targets for new anti-cancer drug development. Mol Cancer 2017;16:153 [PubMed: 28927416]
44. Jones VS, Huang RY, Chen LP, Chen ZS, Fu L, Huang RP. Cytokines in cancer drug resistance: Cues to new therapeutic strategies. Biochim Biophys Acta 2016;1865:255–65 [PubMed: 26993403]
45. Zhang H, Bajraszewski N, Wu E, Wang H, Moseman AP, Dabora SL, et al. PDGFRs are critical for PI3K/Akt activation and negatively regulated by mTOR. J Clin Invest 2007;117:730–8 [PubMed: 17290308]
46. Simon AR, Takahashi S, Severgnini M, Fanburg BL, Cochran BH. Role of the JAK-STAT pathway in PDGF-stimulated proliferation of human airway smooth muscle cells. Am J Physiol Lung Cell Mol Physiol 2002;282:L1296–304 [PubMed: 12003786]
47. Heldin CH. Targeting the PDGF signaling pathway in tumor treatment. Cell Commun Signal 2013;11:97 [PubMed: 24359404]
48. Di Veroli GY, Fornari C, Wang D, Mollard S, Bramhall JL, Richards FM, et al. Combenefit: an interactive platform for the analysis and visualization of drug combinations. Bioinformatics 2016;32:2866–8 [PubMed: 27153664]
49. Huang W, Hickson LJ, Eirin A, Kirkland JL, Lerman LO. Cellular senescence: the good, the bad and the unknown. Nat Rev Nephrol 2022;18:611–27 [PubMed: 35922662]
50. Fornes O, Castro-Mondragon JA, Khan A, van der Lee R, Zhang X, Richmond PA, et al. JASPAR 2020: update of the open-access database of transcription factor binding profiles. Nucleic Acids Res 2020;48:D87–D92 [PubMed: 31701148]
51. Chou TC, Talalay P. Quantitative analysis of dose-effect relationships: the combined effects of multiple drugs or enzyme inhibitors. Adv Enzyme Regul 1984;22:27–55 [PubMed: 6382953]
52. Yonezawa T, Takahashi H, Shikata S, Liu X, Tamura M, Asada S, et al. The ubiquitin ligase STUB1 regulates stability and activity of RUNX1 and RUNX1-RUNX1T1. J Biol Chem 2017;292:12528–41 [PubMed: 28536267]
53. He X, Li Y, Chen Q, Zheng L, Lou J, Lin C, et al. O-GlcNAcylation and stablization of SIRT7 promote pancreatic cancer progression by blocking the SIRT7-REGgamma interaction. Cell Death Differ 2022;29:1970–81 [PubMed: 35422493]

Author Manuscript Author Manuscript Author Manuscript Author Manuscript

54. Song T, Zou Q, Yan Y, Lv S, Li N, Zhao X, et al. DOT1L O-GlcNAcylation promotes its protein stability and MLL-fusion leukemia cell proliferation. Cell Rep 2021;36:109739 [PubMed: 34551297]
55. Xu L, Ye Y, Tao Z, Wang T, Wei Y, Cai W, et al. O-GlcNAcylation of melanophilin enhances radiation resistance in glioblastoma via suppressing TRIM21 mediated ubiquitination. Oncogene 2024;43:61–75 [PubMed: 37950039]
56. Mandoli A, Singh AA, Jansen PW, Wierenga AT, Riahi H, Franci G, et al. CBFB-MYH11/RUNX1 together with a compendium of hematopoietic regulators, chromatin modifiers and basal transcription factors occupies self-renewal genes in inv(16) acute myeloid leukemia. Leukemia 2014;28:770–8 [PubMed: 24002588]
57. Ma CX, Gao F, Luo J, Northfelt DW, Goetz M, Forero A, et al. NeoPalAna: Neoadjuvant Palbociclib, a Cyclin-Dependent Kinase 4/6 Inhibitor, and Anastrozole for Clinical Stage 2 or 3 Estrogen Receptor-Positive Breast Cancer. Clin Cancer Res 2017;23:4055–65 [PubMed: 28270497]
58. Guillen KP, Fujita M, Butterfield AJ, Scherer SD, Bailey MH, Chu Z, et al. A human breast cancer-derived xenograft and organoid platform for drug discovery and precision oncology. Nat Cancer 2022;3:232–50 [PubMed: 35221336]
59. Zhou W, Sun W, Yung MMH, Dai S, Cai Y, Chen CW, et al. Autocrine activation of JAK2 by IL-11 promotes platinum drug resistance. Oncogene 2018;37:3981–97 [PubMed: 29662190]
60. Fyfe G, Fisher RI, Rosenberg SA, Sznol M, Parkinson DR, Louie AC. Results of treatment of 255 patients with metastatic renal cell carcinoma who received high-dose recombinant interleukin-2 therapy. J Clin Oncol 1995;13:688–96 [PubMed: 7884429]
61. Solal-Celigny P, Lepage E, Brousse N, Reyes F, Haioun C, Leporrier M, et al. Recombinant interferon alfa-2b combined with a regimen containing doxorubicin in patients with advanced follicular lymphoma. Groupe d'Etude des Lymphomes de l'Adulte. N Engl J Med 1993;329:1608–14 [PubMed: 8232429]
62. Liu J, Liu C, Qiu L, Li J, Zhang P, Sun Y. Overexpression of both platelet-derived growth factor-BB and vascular endothelial growth factor-C and its association with lymphangiogenesis in primary human non-small cell lung cancer. Diagn Pathol 2014;9:128 [PubMed: 24972450]
63. Kuzmanov A, Hopfer U, Marti P, Meyer-Schaller N, Yilmaz M, Christofori G. LIM-homeobox gene 2 promotes tumor growth and metastasis by inducing autocrine and paracrine PDGF-B signaling. Mol Oncol 2014;8:401–16 [PubMed: 24423492]
64. Kennedy AL, Morton JP, Manoharan I, Nelson DM, Jamieson NB, Pawlikowski JS, et al. Activation of the PIK3CA/AKT pathway suppresses senescence induced by an activated RAS oncogene to promote tumorigenesis. Mol Cell 2011;42:36–49 [PubMed: 21474066]
65. Thill M, Berna MJ, Kunst F, Wege H, Strunnikova NV, Gordiyenko N, et al. SU5416 induces premature senescence in endothelial progenitor cells from patients with age-related macular degeneration. Mol Vis 2011;17:85–98 [PubMed: 21245959]
66. Miyoshi H, Shimizu K, Kozu T, Maseki N, Kaneko Y, Ohki M. t(8;21) breakpoints on chromosome 21 in acute myeloid leukemia are clustered within a limited region of a single gene, AML1. Proc Natl Acad Sci U S A 1991;88:10431–4 [PubMed: 1720541]
67. Zhang Z, Qiu N, Yin J, Zhang J, Liu H, Guo W, et al. SRGN crosstalks with YAP to maintain chemoresistance and stemness in breast cancer cells by modulating HDAC2 expression. Theranostics 2020;10:4290–307 [PubMed: 32292495]
68. Debaize L, Jakobczyk H, Avner S, Gaudichon J, Rio AG, Serandour AA, et al. Interplay between transcription regulators RUNX1 and FUBP1 activates an enhancer of the oncogene c-KIT and amplifies cell proliferation. Nucleic Acids Res 2018;46:11214–28 [PubMed: 30500954]
69. Yamaguchi Y, Kurokawa M, Imai Y, Izutsu K, Asai T, Ichikawa M, et al. AML1 is functionally regulated through p300-mediated acetylation on specific lysine residues. J Biol Chem 2004;279:15630–8 [PubMed: 14752096]
70. Riddell A, McBride M, Braun T, Nicklin SA, Cameron E, Loughrey CM, et al. RUNX1: an emerging therapeutic target for cardiovascular disease. Cardiovasc Res 2020;116:1410–23 [PubMed: 32154891]

Author Manuscript Author Manuscript Author Manuscript Author Manuscript

71. Zhang H, Lin J, Zheng S, Ma L, Pang Z, Yin H, et al. CDKL3 is a targetable regulator of cell cycle progression in cancers. J Clin Invest 2024;134

72. Gong X, Litchfield LM, Webster Y, Chio LC, Wong SS, Stewart TR, et al. Genomic Aberrations that Activate D-type Cyclins Are Associated with Enhanced Sensitivity to the CDK4 and CDK6 Inhibitor Abemaciclib. Cancer Cell 2017;32:761–76 e6 [PubMed: 29232554]

73. Ono M, Oba T, Shibata T, Ito KI. The mechanisms involved in the resistance of estrogen receptor-positive breast cancer cells to palbociclib are multiple and change over time. J Cancer Res Clin Oncol 2021;147:3211–24 [PubMed: 34244855]

Author Manuscript Author Manuscript Author Manuscript Author Manuscript

Significance:

RUNX1-PDGF-BB signaling drives resistance to CDK4/6 inhibition in breast cancer, providing the foundation to develop approaches to target the RUNX1-PDGF-BB axis to overcome CDK4/6 inhibitor resistance in breast cancer patients.

Author Manuscript
Author Manuscript
Author Manuscript
Author Manuscript

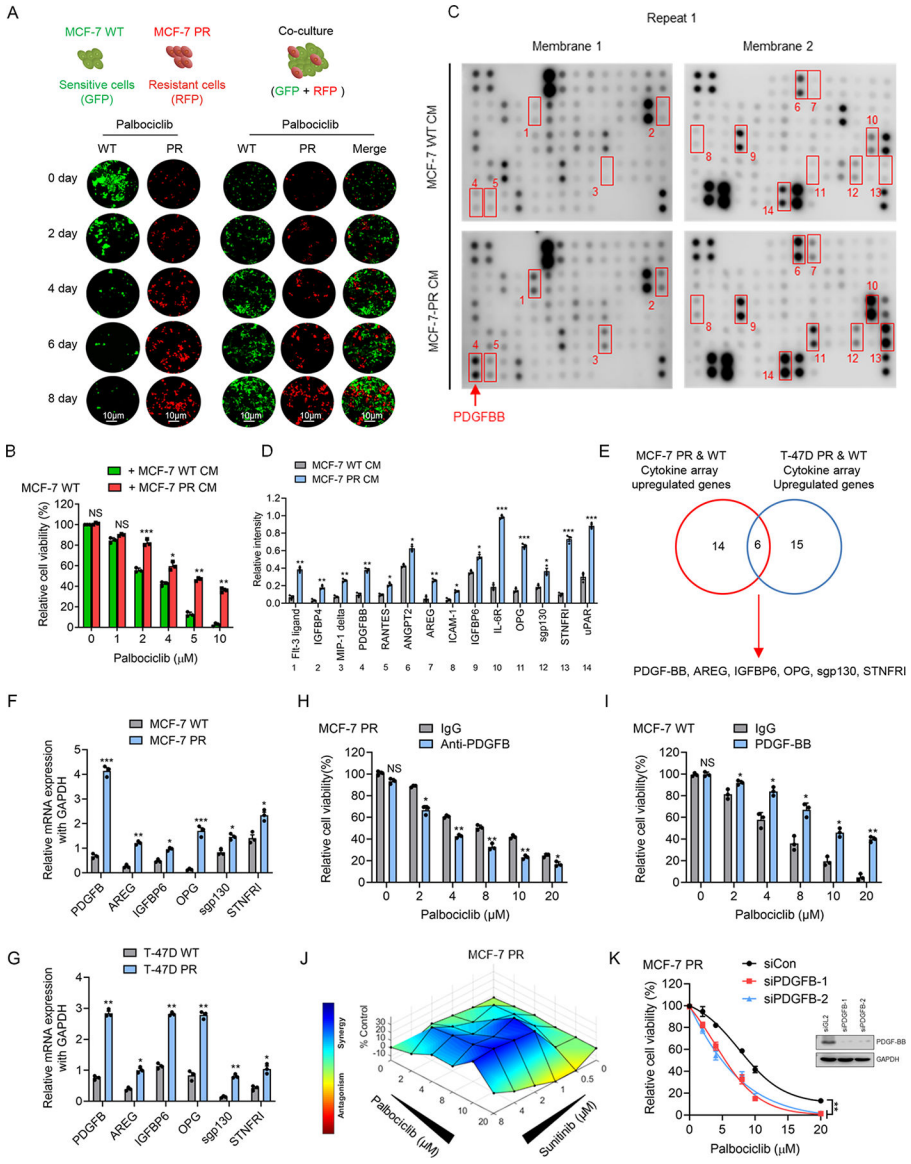

Figure 1. Identification of PDGF-BB that promotes palbociclib-resistance in ER+ breast cancer cells

(**A**) MCF-7 WT-GFP cells and MCF-7 PR-RFP cells were monocultured or co-cultured in the presence of palbociclib (2μM) for 8 days. Images were taken on day 0, day 2, day 4, day 6, and day 8. The scale bar represents 10 μm. (**B**) Viability of MCF-7 WT treated with the indicated amount of conditioned medium (CM) from MCF-7 WT or MCF-7 PR cells for two days, followed by treatment with the indicated concentrations of palbociclib for 3 days. (**C-D**) Representative image (C) and quantification (D) of cytokine arrays showing the expression levels of the indicated upregulated cytokines in the culture medium of MCF-7 WT and MCF-7 PR cells from three independent experiments. The spots highlighted within the red rectangle indicate cytokines that are upregulated in MCF-7 PR CM compared to MCF-7 WT CM. (**E**) The schematic illustrates the overlap of upregulated cytokines identified by the cytokine array from MCF-7 PR & MCF-7 WT CM and T-47D PR & T-47D WT CM. (**F-G**) MCF-7 WT/MCF-7 PR cells (F) and T-47D WT/T-47D PR cells (G)

Author Manuscript Author Manuscript Author Manuscript Author Manuscript

were harvested and then subjected to qPCR to examine the mRNA levels of the indicated genes. (**H)** Cell viability was assessed in MCF-7 PR cells treated with 1 μg/mL PDGFB neutralizing antibody or IgG, in combination with increasing concentrations of palbociclib, for 3 days. (**I**) Cell viability was examined in MCF-7 WT cells treated with 100ng/mL recombinant PDGF-BB protein or IgG, in combination with increasing concentrations of palbociclib, for 3 days. (**J**) Surface plots show the synergy between palbociclib and sunitinib in MCF-7 PR cells ($n = 3$). (**K**) MCF-7 PR cells were transfected with the indicated siRNAs for 48 hr, then cell viability was examined with indicated concentrations of palbociclib for 3 days. Data are presented as mean ± SEM. Statistic analysis was performed by GraphPad Prism 9.5.0 using Welch's *t*-test for the data shown in (D, F, G), using Multiple *t*-tests followed by Holm–Sidak correction for the data shown in (B, H, I, K). $*P \leq 0.05$, $**P \leq 0.01$, $***P \leq 0.001$; "NS" indicates no significant difference.

Author Manuscript Author Manuscript Author Manuscript Author Manuscript

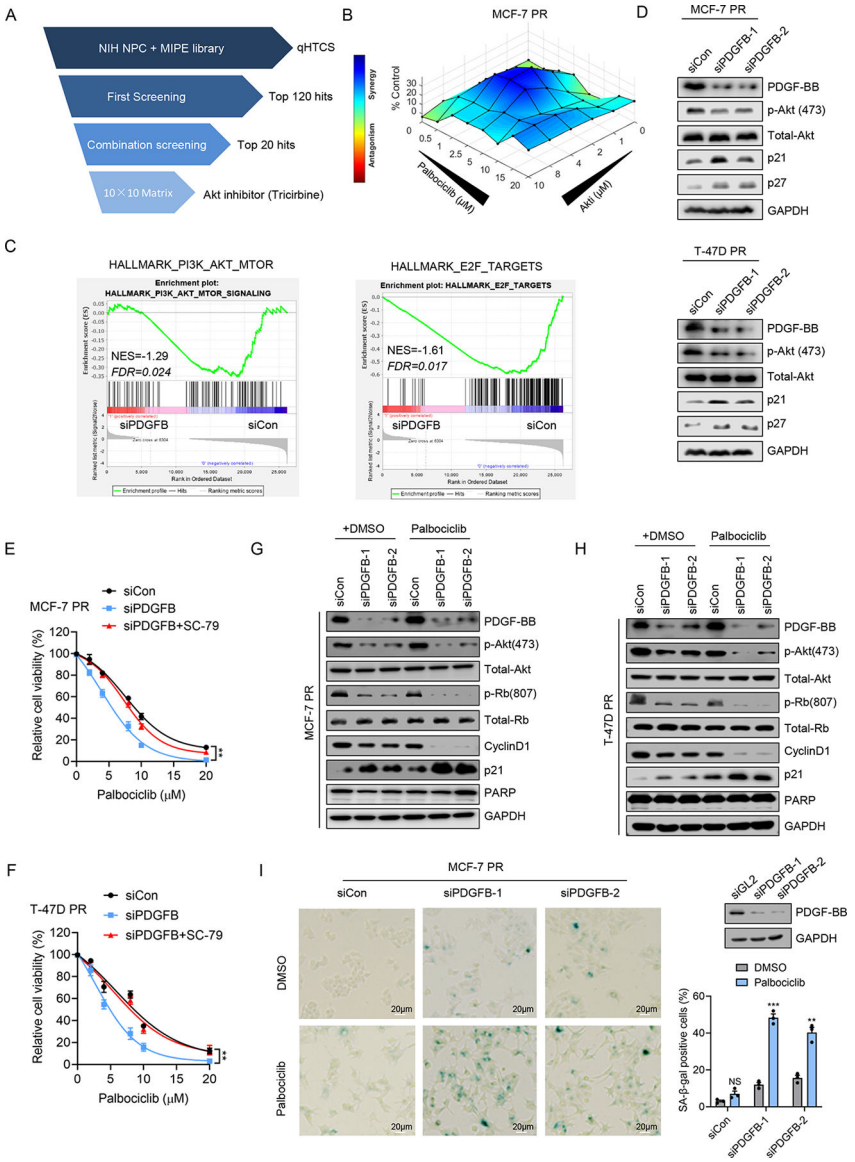

Figure 2. Inhibition PDGF-BB overcomes palbociclib resistance by inhibiting Akt and activating the senescence pathway in breast cancer cells

(**A**) Schematic of qHTCS to identify Akti (Tricirbine) that can overcome palbociclib resistance. (**B**) Surface plots showing the synergy between palbociclib and Tricirbine in MCF-7 PR cells ($n = 3$). (**C**) GSEA profiling shows the enrichment of the PI3K_Akt_MTOR geneset and E2F geneset in MCF7 PR cells treated with siCon or si-PDGF-BB. NES scores and FDR values were determined by GSEA software. (**D**) MCF-7 PR cells (top) and T-47D PR cells (bottom) were transfected with indicated siRNA for 48 hr, cells were then harvested and immunoblotted for the indicated proteins. (**E-F**) MCF-7 PR cells (E) and T-47D PR cells (F) were pretreated with/without SC-79 for 24h, then transfected with the indicated siRNAs for 48h, and cell viability was examined with the indicated concentrations of palbociclib for 3 days. (**G-H**) MCF-7 PR cells (G) and T-47D PR cells (H) were transfected with indicated siRNA for 24h and then treated with 4 μM Palbociclib for 2 days, then cell lysed were harvested and immunoblotted for indicated proteins. (**I**) Representative images

Author Manuscript Author Manuscript Author Manuscript Author Manuscript

of SA-β-gal staining in MCF-7 PR cells transfected with the indicated siRNA for 24 hours, followed by treatment with 4 μM Palbociclib for 4 days. The scale bar represents 20 μm. All data are presented as mean ± SEM and analyzed by Multiple *t*-tests followed by Holm–Sidak correction in GraphPad Prism 9.5.0. $^{**}P \leq 0.01$, $^{***}P \leq 0.001$; "NS" indicates no significant difference.

Author Manuscript Author Manuscript Author Manuscript Author Manuscript

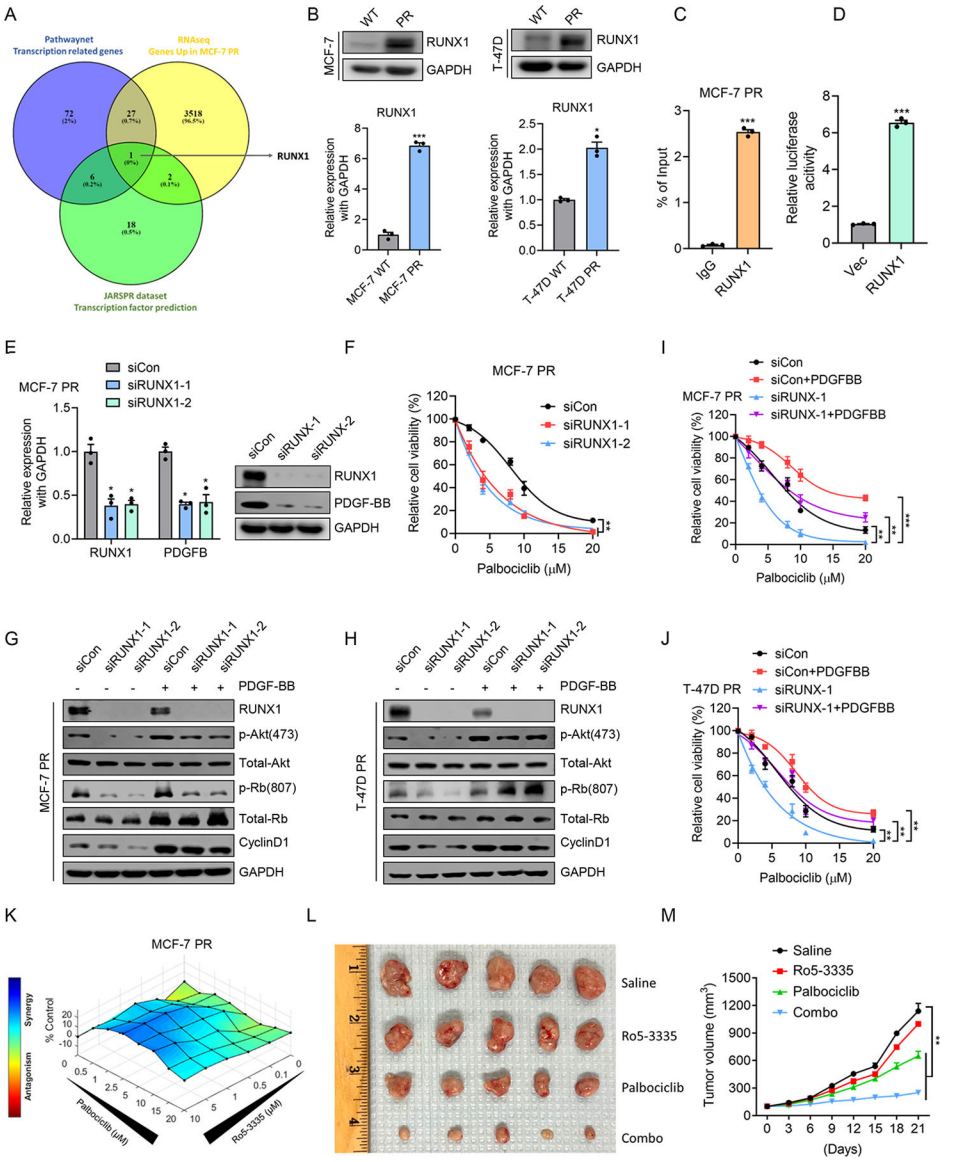

Figure 3. RUNX1 transactivates PDGF-BB in palbociclib-resistant breast cancer cells

(**A**) Venn diagram showing the overlap of transcription-regulated genes with PDGF-BB from PathwayNet, transcription factors targetting the promoter region of PDGF-BB by JARSPR database, and genes upregulated from RNA-seq analysis in MCF-7 PR cells. (**B**) MCF-7 WT & PR cells (left) and T-47D WT & PR cells (right) were harvested and then subjected to qPCR and immunoblotting to examine the expression of the indicated genes and proteins. (**C**) ChIP-qPCR was employed to examine the binding of RUNX1 to the promoter region of the PDGFB. (**D**) Luciferase reporter assay was performed to examine the transcription activities of RUNX1 in MCF-7 PR cells. Renilla luciferase plasmid was used as an internal control. (**E**) MCF-7 PR cells were transfected with the indicated siRNAs for 48 hr, then cells were harvested and then subjected to qPCR and immunoblotting to examine the expression of indicated genes. (**F**) MCF-7 PR cells were transfected with the indicated siRNAs for 48 hr, then cell viability was examined with indicated concentrations of palbociclib for 3 days.

Author Manuscript Author Manuscript Author Manuscript Author Manuscript

(**G-H**) MCF-7 PR cells (G) and T-47D PR cells (H) were transfected with indicated siRNA for 24h, and then incubated with/without recombinant PDGF-BB (100ng/mL) for 48h, cells were then harvested and immunoblotted for the indicated proteins. (**I-J**) MCF-7 PR cells (I) and T-47D PR cells (J) were transfected with indicated siRNA for 24 hrs, followed by incubation with or without recombinant PDGF-BB (100 ng/mL) in combination with the indicated concentrations of palbociclib for 3 days. (**K**) Surface plots show the synergy between palbociclib and Ro5-3335 in MCF-7 PR cells. (**L-M**) Representative images (L) and growth curves (M) of MCF-7 PR xenograft tumors with the indicated treatments for 3 weeks (n = 5 mice/group). Palbociclib and RUNX1 inhibitor Ro5-3335 were administered intraperitoneally every 2 days for 3 consecutive weeks at a dose of 25 mg/kg and 10 mg/kg, respectively. The data in (M) are presented as mean ± SD, whereas data in (B-F, I-J) are shown as mean ± SEM. Statistic analysis was performed by GraphPad Prism 9.5.0 using Welch's *t*-test for the data shown in (B-E), using Multiple *t*-tests followed by Holm–Sidak correction for the data shown in (F, I, J, M). $*P \leq 0.05$, $**P \leq 0.01$, $***P \leq 0.001$.

Author Manuscript Author Manuscript Author Manuscript Author Manuscript

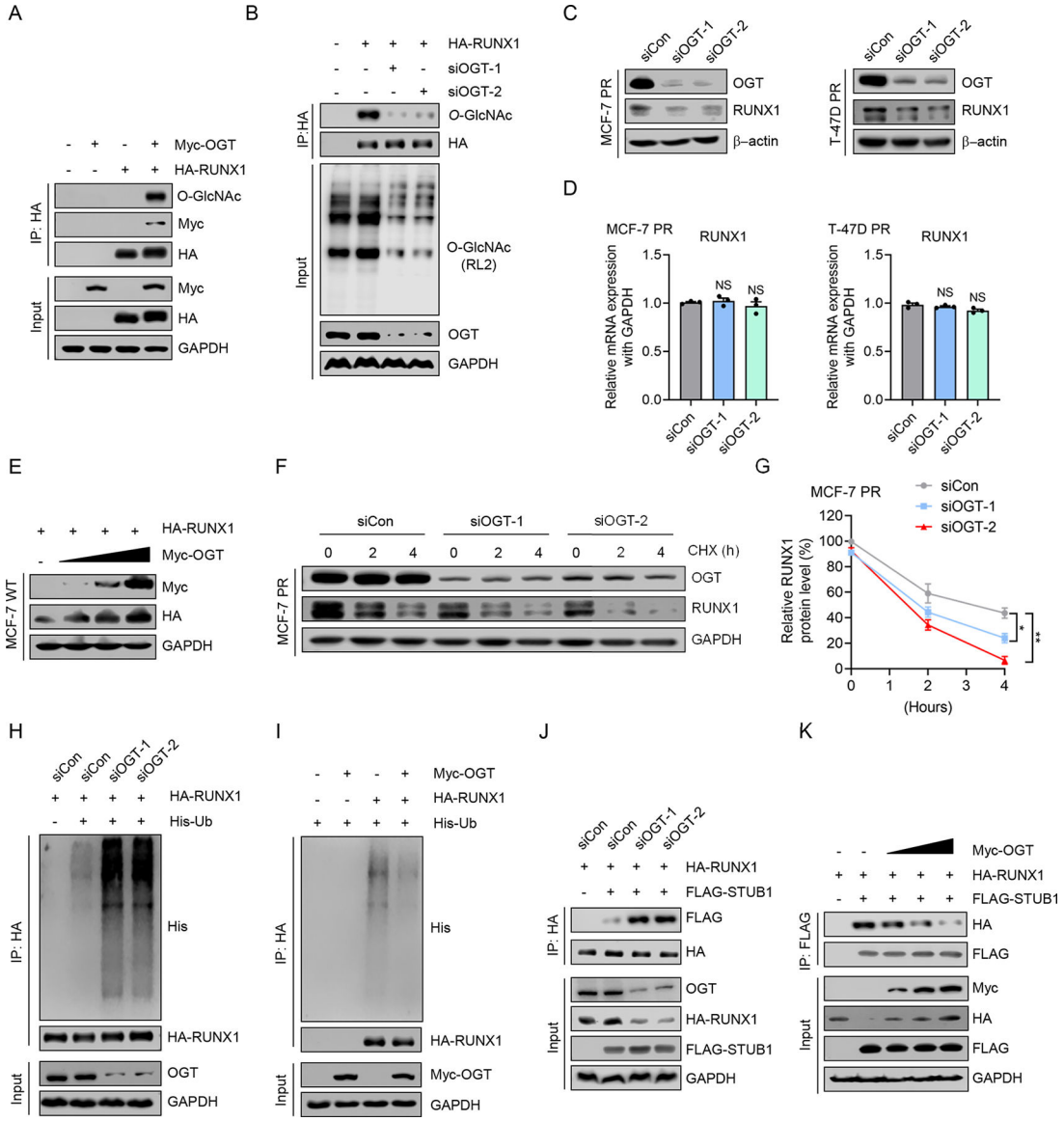

Figure 4. O-GlcNAcylation of RUNX1 by OGT stabilizes RUNX1 by preventing STUB1-mediated ubiquitination

(**A**) MCF-7 WT cells were transfected with the indicated plasmids for 48 hr before being harvested for co-IP assay. HA-IPs were immunoblotted for indicated proteins. (**B**) MCF-7 PR cells were transfected with the indicated siRNAs and plasmids for 48 hr before being harvested. FLAG-IPs were immunoblotted for the indicated proteins. (**C-D**) MCF-7 PR cells and T-47D PR cells were transfected with the indicated siRNAs for 48 hr before being harvested. Cell lysates were then subjected to immunoblotting for the indicated proteins and qPCR to examine mRNA levels of the indicated genes. (**E**) MCF-7 WT cells were transfected with the indicated plasmids for 48 hr before being harvested. Cell lysates were then subjected to immunoblotting for the indicated proteins. (**F-G**) MCF-7 PR cells were transfected with indicated siRNA for 48 hr, followed by treatment with CHX (100μg/mL) for the indicated time points, and then subjected to immunoblotting for the indicated proteins and quantification of the protein levels. (**H**) HEK293T cells were transfected

Author Manuscript Author Manuscript Author Manuscript Author Manuscript

with the indicated siRNAs and plasmids for 48 hr before being harvested. HA-IPs were immunoblotted for the indicated proteins. (**I**) HEK293T cells were transfected with the indicated plasmids for 48 hr before being harvested. HA-IPs were immunoblotted for the indicated proteins. (**J**) HEK293T cells were transfected with the indicated siRNAs and plasmids for 48 hr before being harvested. HA-IPs were immunoblotted for the indicated proteins. (**K**) HEK293T cells were transfected with the indicated plasmids for 48 hr before being harvested. FLAG-IPs were immunoblotted for the indicated proteins. The data in (D) are presented as mean ± SEM, whereas data in (G) are shown as mean ± SD. Statistic analysis was performed by GraphPad Prism 9.5.0 using Welch's *t*-test for the data shown in (D), using Multiple *t*-tests followed by Holm–Sidak correction for the data shown in (G). $*P \leq 0.05$, $**P \leq 0.01$; "NS" indicates no significant difference.

Author Manuscript Author Manuscript Author Manuscript Author Manuscript

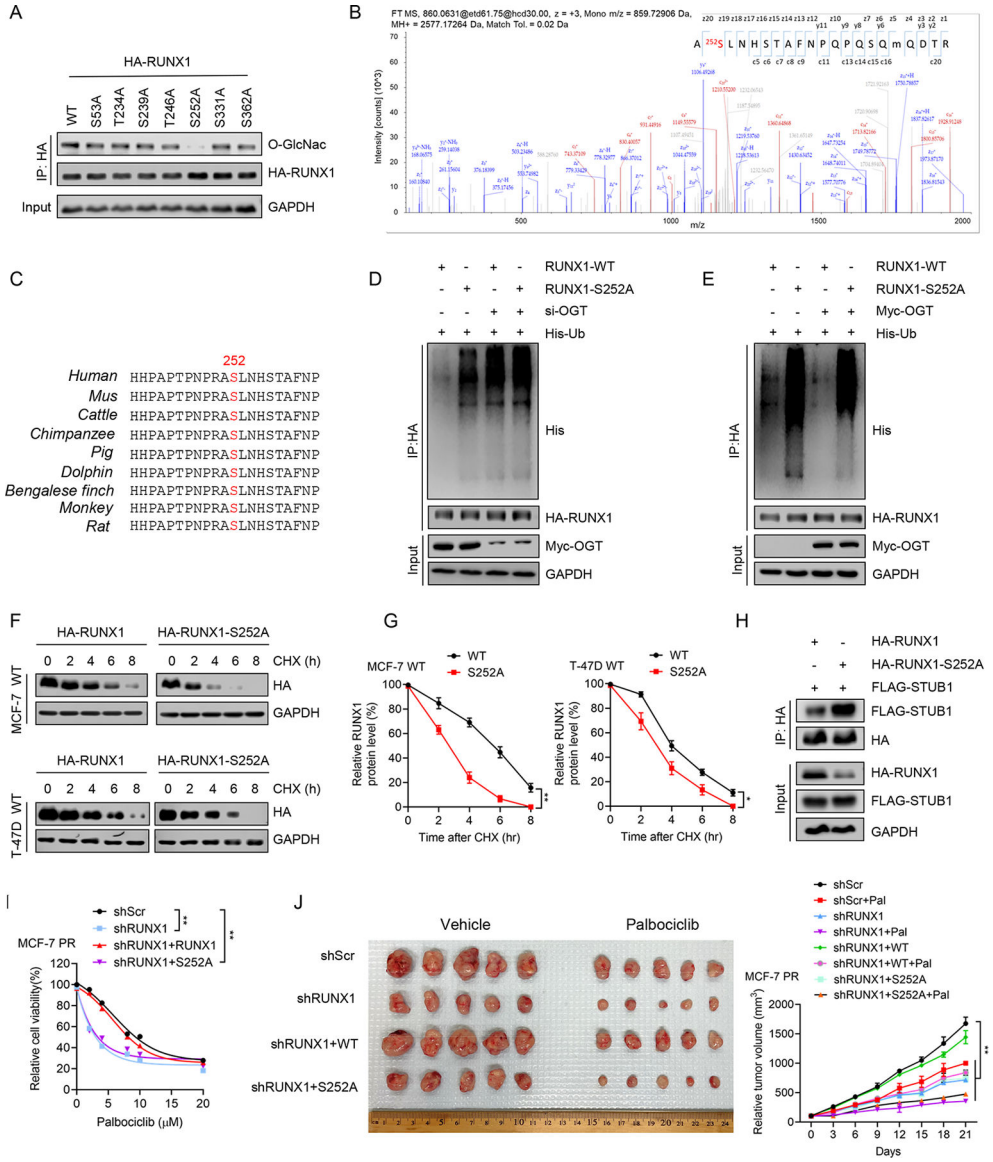

Figure 5. O-GlcNAcylation of RUNX1 at Serine 252 is required for its stability and palbociclib-resistance

(**A**) HEK293T cells expressing RUNX1 or its O-GlcNAc mutants from plasmids were harvested 48 hr after transfection, followed by co-IP. HA-IPs were then immunoblotted for the indicated proteins. (**B**) HA-RUNX1 and Myc-OGT were co-expressed in HEK293T cells, then HA-RUNX1 was purified and analyzed by nanoUPLC-MS/MS to identify O-GlcNAc sites with the annotated mass spectrum (S252 O-GlcNAcylation is illustrated; matched b, y, c, z fragments are highlighted; the modified residue is showed in red; m, methione oxidation). (**C**) The RUNX1 S252 site is conserved across various species. (**D-E**) HEK293T cells were transfected with the indicated siRNAs and plasmids for 48 hr before being harvested. HA-IPs were immunoblotted for the indicated proteins. (**F-G**) MCF-7 WT cells and T-47D WT cells were transfected with RUNX1 WT or RUNX1 S252A mutant plasmids for 48 hr, followed by treatment with CHX (50μg/mL) for the indicated time points, and then subjected to immunoblotting for the indicated proteins and quantification of

Author Manuscript Author Manuscript Author Manuscript Author Manuscript

the protein levels. (**H**) HEK293T cells were transfected with the indicated plasmids for 48 hr before being harvested. HA-IPs were immunoblotted for the indicated proteins. (**I**) MCF-7 PR cells were transfected with shRUNX1 and selected with 2ug/ml puromycin for 2 weeks. Cells were then transfected with RUNX1-WT or RUNX1-S252A plasmids, followed by examination of viability after treatment with the indicated concentrations of palbociclib for 3 days. (**J**) Representative images (left) and growth curves (right) of MCF-7 PR xenograft tumors with the indicated treatments for 3 weeks (n = 5 mice/group). Palbociclib was administered intraperitoneally every 2 days for 3 consecutive weeks at a dose of 25 mg/kg. The data in (G, J) are presented as mean ± SD, whereas data in (I) are shown as mean ± SEM. Statistic analysis was performed using Multiple *t*-tests followed by Holm–Sidak correction in GraphPad Prism 9.5.0. $*P \leq 0.05$, $**P \leq 0.01$.

Author Manuscript Author Manuscript Author Manuscript Author Manuscript

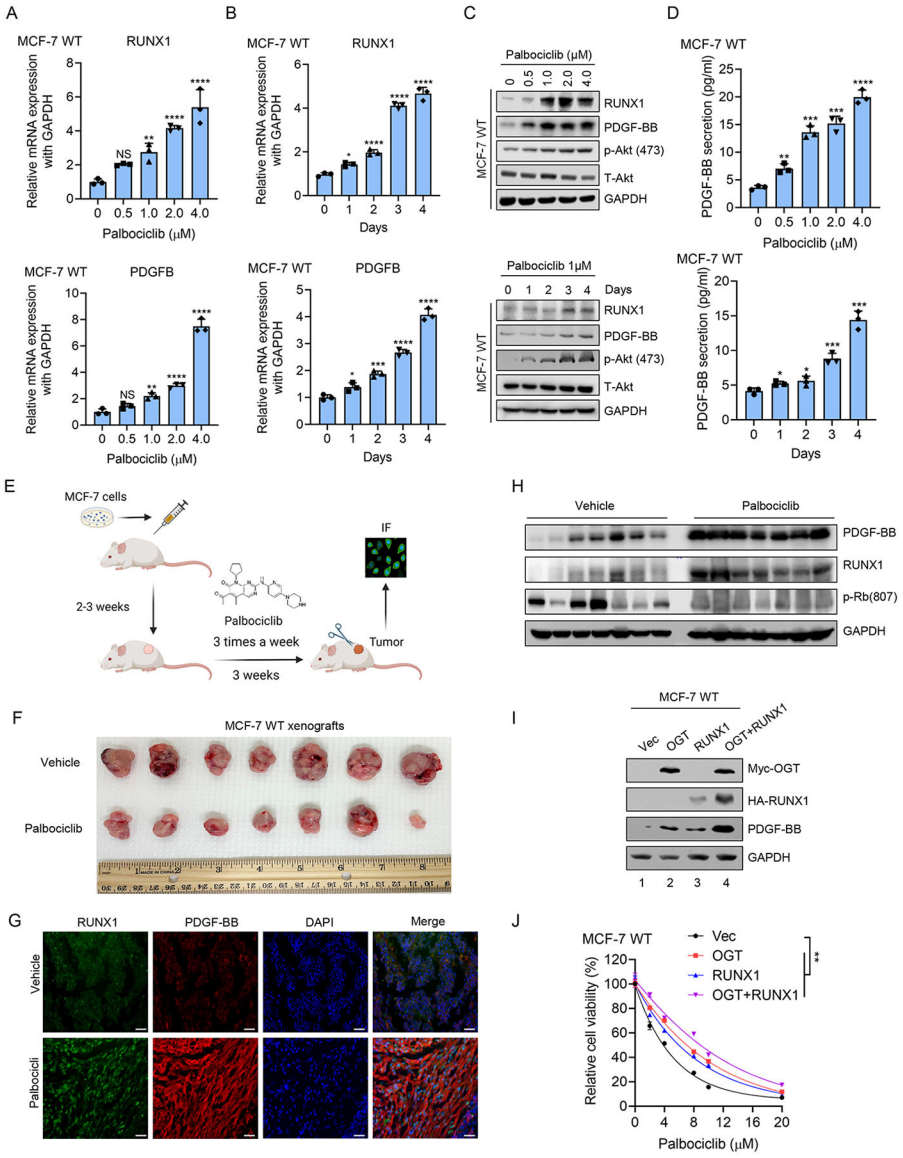

Figure 6. Palbociclib treatment activates the RUNX1-PDGF-BB axis both *in vitro* and *in vivo*

(**A-B**) MCF-7 WT cells were treated with various doses of palbociclib for 4 days (A) or with 1μM palbociclib for different durations (B). The cells were then lysed, and qPCR was performed to analyze the mRNA levels of the indicated genes. (**C**) MCF-7 WT cells were collected after the indicated treatments for 4 days and then subjected to immunoblotting for the indicated proteins. (**D**) MCF-7 WT cell culture medium was collected after the indicated treatment for 4 days for examination of secreted PDGF-BB levels by ELISA. (**E**) A schematic presentation of the experiments presented in F-H. (**F**) Representative images of MCF-7 WT xenograft tumors with intraperitoneal palbociclib treatment every 2 days for 3 consecutive weeks at a dose of 10mg/kg (n = 7 mice/group). (**G-H**) MCF-7 WT xenograft tumor tissues were collected after the indicated treatments for 3 weeks, and then subjected to immunostaining (G) and immunoblotting for the indicated proteins (H). (**I**) Western Bloting shows increased PDGF-BB protein levels in MCF-7 WT cells with overexpression of OGT,

Author Manuscript Author Manuscript Author Manuscript Author Manuscript

RUNX1, or OGT and RUNX1 together. (**J**) Cell viability of the cells treated in (I). Data are presented as mean ± SEM and analyzed by Multiple *t*-tests followed by Holm-Sidak correction in GraphPad Prism 9.5.0. *$P \leq 0.05$, **$P \leq 0.01$, ***$P \leq 0.001$, ****$P \leq 0.0001$; "NS" indicates no significant difference.

Author Manuscript Author Manuscript Author Manuscript Author Manuscript

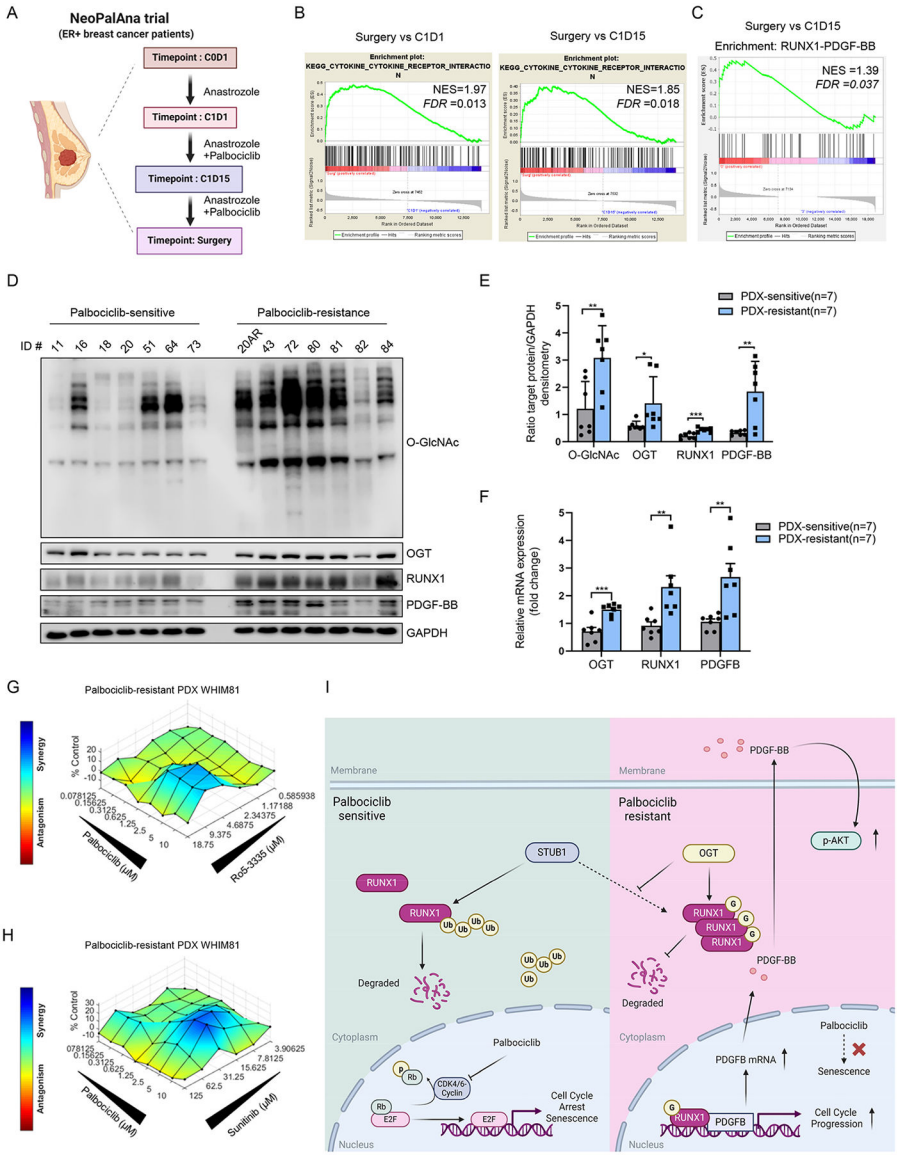

Figure 7. RUNX1-PDGF-BB axis is upregulated in breast cancer patients treated with palbociclib

(A) Schematic of NeoPalAna Trial for ER$^+$ breast cancer patients. (**B**) GSEA profiling showing the enrichment of the Cytokine_Receptor_Interaction geneset in the Surgery group vs. C1D1 group and Surgery group vs. C1D15 group; **(C)** The enrichment of the RUNX1-PDGF-BB signature geneset in the Surgery group vs. C1D15 group. NES scores and FDR values were determined by GSEA software. (**D**) Palbociclib-resistant and sensitive breast cancer PDX lines were collected and subjected to Western blotting. (**E**) Quantification results of the indicated proteins. (**F**) Palbociclib-resistant and sensitive breast cancer PDX lines were collected and subjected to qPCR to examine the mRNA levels of the indicated genes. (**G-H)** Surface plots to exhibit the synergy between palbociclib and Ro5-3335 (G) as well as palbociclib and sunitinib (H) in palbociclib-resistant organoid cells derived from the PDX line WHIM81 (n = 3). (**I**) Schematic representation of how O-GlcNAcylation of RUNX1 regulates PDGF-BB signaling and palbociclib resistance in breast cancer cells. See

Author Manuscript Author Manuscript Author Manuscript Author Manuscript

text for details. The data in (E) are presented as mean ± SD, whereas data in (F) are shown as mean ± SEM. Statistic analysis was performed using Welch's *t*-test in GraphPad Prism 9.5.0. *$P \leq 0.05$, **$P \leq 0.01$, ***$P \leq 0.001$.